1

Controllable Self-Assembly of One-Dimensional Nanocrystals

Shaoyi Zhang, Yang Yang, and Zhihong Nie

University of Maryland, Department of Chemistry and Biochemistry, 8051 Regents Drive, College Park, MD 20742, USA

1.1 Introduction

In the past decades, controlled assembly of nanocrystals (NCs) has been a topic of continuous interest. The tremendous interest in organizing NCs mainly stemmed from the potential applications of NCs in diverse areas, including chemical and biological sensing, energy storage and production, and optoelectronic devices. Recent advances at this frontier are also partially driven by the rapid development in the synthesis of relatively monodispersed NC building blocks with controlled size, shape, and composition [1, 2]. Compared to spherical NCs, one dimensional (1D) NCs, that is, nanorods (NRs) and nanowires (NWs), exhibit unique optical, electronic, and magnetic properties due to their shape anisotropy [3, 4]. Taking Au NRs as an example, they exhibit localized surface plasmon resonance (LSPR) and strong photothermal effect, which enable their broad applications in such areas as cancer imaging and therapy. The LSPR absorption of these NRs can be tailored in the range from visible to near-infrared wavelengths for specific applications by controlling the aspect ratio of NRs. To date, various methods have been developed for the organization of 1D NCs into functional structures. In particular, the bottom-up assembly approach offers a more robust, scalable, and cost-effective way to fabricate arrays of NCs in a controlled manner, compared to top-down techniques such as electron-beam and focused-ion beam lithography [5]. In this chapter, we have classified the current self-assembly methods into four major categories, namely templated assembly, field-driven assembly, assembly at interfaces, and ligand-guided assembly. The following section features the properties and applications of assemblies of 1D NCs. Finally, conclusion and outlook are presented in the last section.

Functional Organic and Hybrid Nanostructured Materials: Fabrication, Properties, and Applications,
First Edition. Edited by Quan Li.

1.2 Assembly Strategies

1.2.1 Templated Assembly

Templated assembly, as the name implies, is the assembly directed by a predesigned template, which governs the anchoring of NCs on (or within) the template. As a straightforward method, the geometry and patterning of templates or the distribution of functional groups on the template dictates the location, orientation, or alignment of NCs as well as the association state of NCs. Typically, the templating effect arises from physical confinement of the template, differential affinity of NCs toward the template surface, or chemical bonding between the ligands on NCs and templates. Recent progress in this frontier has allowed the assembly of 1D NCs into long-range-ordered structures with high yield and well-defined orientation of NCs at single-particle resolution. This largely fulfills the requirement of assemblies on substrates for applications including biosensors, optical devices, metamaterials, and so on [6]. In this section we discuss several categories of assembly systems, classified on the basis of the characteristics of templates.

1.2.1.1 Geometrically Patterned Template

Assembly based on geometrically patterned template utilizes the topographical patterns on a substrate to direct the interaction and shape-selective organization of NCs within the patterns. Representative topographical patterns include periodic polygonal grooves, discrete spherical poles, and parallel channels. These templates are usually fabricated by top-down approaches such as photolithography, chemical vapor deposition, inkjet printing, and focused beam (electrons, ions, laser, etc.) etching [7]. To achieve the desired assembly structures of NCs, the geometric parameters (e.g., size, depth, and geometry of patterns) have to be carefully tuned. By using this method, various types of assemblies have been produced, such as discrete clusters, 1D arrays, 2D monolayers, and 3D supercrystals.

Toward the end of the last century, Blaaderen *et al*. reported the crystallization of bulk colloidal crystals through the slow sedimentation of silica spheres onto a pole-patterned poly(methyl methacrylate) (PMMA) layer [8]. Xia *et al*. fabricated a series complex aggregates of polystyrene beads including polygonal or polyhedral clusters, linear or zigzag chains, and circular rings by combing physical templating and capillary forces [9]. Thanks to the developments in pattern design, great progress has been achieved in fabricating diverse arrays of 1D NCs on patterned substrates with high yield, good scalability, and superior morphology control [10]. Bach *et al*. produced free-standing arrays of hexagonal close-packed Au NRs on predefined locations using a patterned substrate containing square grooves of different wettability on the surface of the substrate [11]. Recently, Brugger *et al*. realized the capillary assembly of Au NRs into large-area ordered structures on substrates with predetermined surface patterns [12]. In a typical capillary assembly, the colloidal solution is confined between a patterned substrate and a sliding top plate. The receding meniscus directs the colloidal solution to move over the substrate in a controlled manner. Subsequently, NCs

assemble from the three-phase contact line at predetermined assembly sites. In order to improve the accuracy and success rate in the placement of NCs, it is crucial to prevent the possible removal of NCs that are inserted in the traps. In this work, the precise control over the organization of Au NRs on the substrate was accomplished by the delicate design of the geometry of the traps. As shown in Figure 1.1, funneled traps with auxiliary sidewalls were fabricated to effectively prevent the removal of NRs after their insertion into the traps. With the introduction of sidewalls, the assembly yield goes up to 100%. The positional control of Au NRs goes down to the nanometer scale. As shown in Figure 1.1b, Au NRs can be selectively placed onto a substrate with arbitrary patterns by using this method.

Apart from directly modulating the patterns on a substrate, confinement can be used to control the organization of NCs. Typically, a suspension of NCs is confined between a topologically patterned template at the top and a

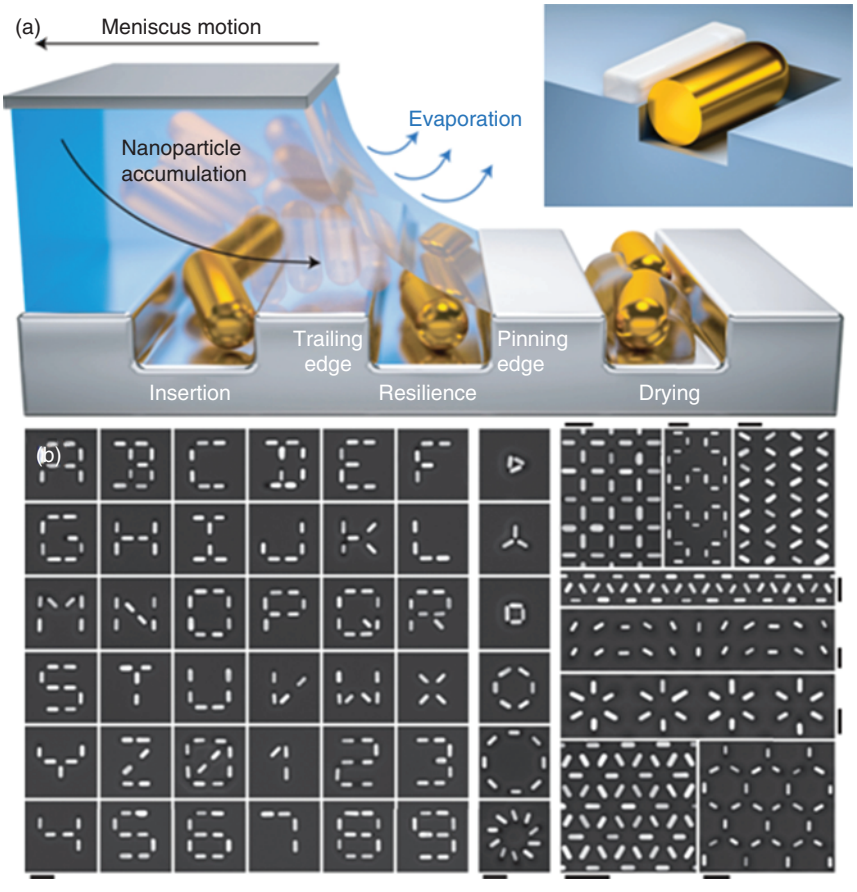

Figure 1.1 Assembly of Au NRs on a patterned solid substrate. (a) Scheme of capillary assembly of Au NRs onto substrates with geometrical patterns. (b) SEM images of Au NRs patterns by topographically templated capillary assembly. Scale bar: 250 nm. (Flauraud *et al*. 2016 [12]. Reproduced with permission of Nature Publishing Group.)

smooth substrate at the bottom. The subsequent evaporation of solvent in a controlled manner drives the formation of an orientated array of NCs. The above templates function as both regulating the solvent evaporation and controlling the deposition of NCs at given locations on the substrate. Typical templates such as the elastomeric poly(dimethyl siloxane) (PDMS) stamp and highly oriented pyrolytic graphite (HOPG) have been employed to provide confinement to facilitate the formation of closely packed arrays of 1D NCs [13]. In this case, the templates can be easily removed and recycled while the assemblies are left on flat substrates. As an example, Ahmed *et al*. reported the formation of perpendicular superlattices of hexagonally oriented CdS NRs using an HOPG template [14]. A dispersion of CdS NRs in toluene was trapped between a block of HOPG and a smooth silicon wafer. Upon slow evaporation of the solvent, a large-area ($\sim$2 μm^2) monolayer of perpendicularly oriented NRs was formed on the substrate. It was found that the monodispersity and hexagonal facets along the *c*-axis of wurtzite NRs are crucial to the formation of highly ordered lattices. Also, the cleaved surface of the HOPG substrate efficiently trapped the NRs in a narrow capillary, facilitating the slow evaporation of solvents. Later, Liz-Marzan *et al.* reported a simple assembly method to produce large-area (up to millimeter size) supercrystal arrays of Au NRs using a patterned PDMS mold [15]. The supercrystals with tunable size, shape, and height exhibited homogeneous and intense electric field enhancement over the entire assemblies for effective surface-enhanced Raman spectroscopy (SERS) detection.

The assembly strategy using geometrically patterned templates allows the fabrication of large-area, predetermined assembly structures with controlled geometric parameters. These assemblies of NCs can be readily integrated with a device supported on a substrate and tailored for a broad range of applications such as sensors and optoelectronics by designing the templates. To facilitate the interaction between the template and NCs, this method often requires the surface modification of NCs with designed small or large molecules via methods such as ligand exchange.

1.2.1.2 Chemically Patterned Template

Chemically patterned templates such as carbon nanotubes (CNTs), polymer matrices, and peptide nanostructures have been extensively explored for guiding the assembly of 1D NCs. In this method, the organization of the NCs is determined by the spatial arrangement of the chemical functional groups that have strong affinity toward NCs. This approach enables the control of not only the position and orientation of NCs with single-particle precision but also the formation of NC arrays in a 3D space. We exclude assembly templated by DNA nanostructures in this section and leave this topic in the section on ligand-guided assembly.

In the simplest scenario, 1D nano- or micro-structures (e.g., CNT, nanofibers, etc.) can be used to template the linear organization of 1D NCs. For example, CNTs are appealing templates for guiding the linear organization of 1D NCs due to their intrinsic mechanical properties and intensively explored surface modifications. The first example of CNT-templated assembly of Au NRs was reported by Liz-Marzan and coworkers [16]. In this work, multiwalled CNTs

were wrapped with poly(styrene sulfonate), followed by the deposition of positively charged poly(diallyldimethyl)ammonium chloride on the surface of CNTs. Au NRs modified with negatively charged poly(vinyl pyrrolidone) (PVP) were organized end to end into stripes on opposite sides of the CNTs as a result of the electrostatic attraction between NRs and CNTs. The end-to-end organization of Au NRs was attributed to the anisotropic surface of NRs and a higher electric potential reduction at the NR tips with high curvature than that at the side of NRs. The organization of NRs need not necessarily be end to end to form simple chains when the template possesses more complex structures. As an interesting example, chiral ribbons assembled from peptides were used to template the side-by-side arrangement of Au NRs into single helical chiral arrays [17]. At the early stage of assembly, spherical NPs were bound to the outer face of the helical ribbon. The *in situ* anisotropic growth of NPs in the presence of peptide conjugates was limited by the width of the helical ribbon, leading to the formation of a parallel array of rod-like particles.

Polymer matrices such as phase-separated block copolymer (BCP) films present a typical class of versatile organic templates for the assembly of 1D NCs [18]. For assembly in a homopolymer matrix, the dispersion and assembly of NCs can be mediated by a series of parameters such as volume content of NCs, the type and length of ligands on NCs, and the length and compatibility of the polymer matrix [19, 20]. With increasing complexity, the majority of these polymeric templates are fulfilled with BCPs that are capable of assembling into a rich variety of nanoscale morphologies in both solutions and films. NCs can be selectively incorporated into one of the phase-segregated nanoscale domains, depending on the miscibility between the NCs (or ligands on NCs) and the BCP block of the host phase. Generally, the spatial placement of 1D NCs can be realized by controlling the length and chemical moieties of each block of BCPs [21]. In one example reported by Zhu and Nie's groups, Au NRs assembled in an end-to-end or a side-by-side manner within cylindrically confined nanodomains of BCPs [22]. As shown in Figure 1.2, assemblies of the

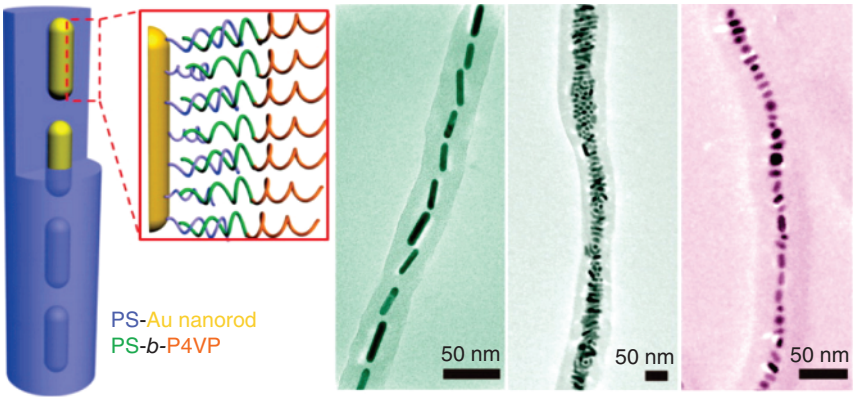

Figure 1.2 Schematic illustration of Au NRs assembled in an end-to-end or a side-by-side manner within cylindrically confined nanodomains of BCPs. (Liu *et al*. 2013 [22]. Reproduced by permission from American Chemical Society.)

supramolecular copolymer formed by PS-*b*-poly(4-vinylpyridine) (PS-*b*-P4VP) and 3-*n*-pentadecylphenol (PDP) were used to template the organization of Au NRs tethered with PS chains with two different lengths. The NRs were effectively organized in the cylindrical PS domains. Because of the reversible hydrogen bonding between the 4-vinylpyridine units of P4VP and the phenol group of PDP, the supramolecular matrix could be disassembled into isolated cylindrical micelles consisting of a PS-tethered Au NR core and a P4VP shell. The arrangement of NRs within the cylinders is largely determined by the diameter of cylindrical PS phase and the aspect ratio and content of NRs. For instance, when the content of Au NR increases gradually, the association of NRs changes from the end-to-end to the twisted side-by-side arrangement.

Chemical patterns generated by phase-separated BCPs on a substrate can be used to selectively absorb and organize NCs. In an early work by Russell and coworkers, a PS-*b*-PMMA film with channels or pores on a silicon wafer was used as a template to guide the assembly of poly(ethylene oxide) (PEO)-functionalized CdSe NRs (Figure 1.3) [23]. The PEO ligand drove the CdSe NRs to migrate from solution to the water/air interface, facilitating the absorption of NRs into the hydrophilic channels or poles of the BCP template. As a result, CdSe NRs were found to align along the channel walls or aggregated in the pores. Later, more advances were made to manipulate the orientation and spacing of NRs by tuning the particle–template and/or particle–particle interactions [22, 24–26].

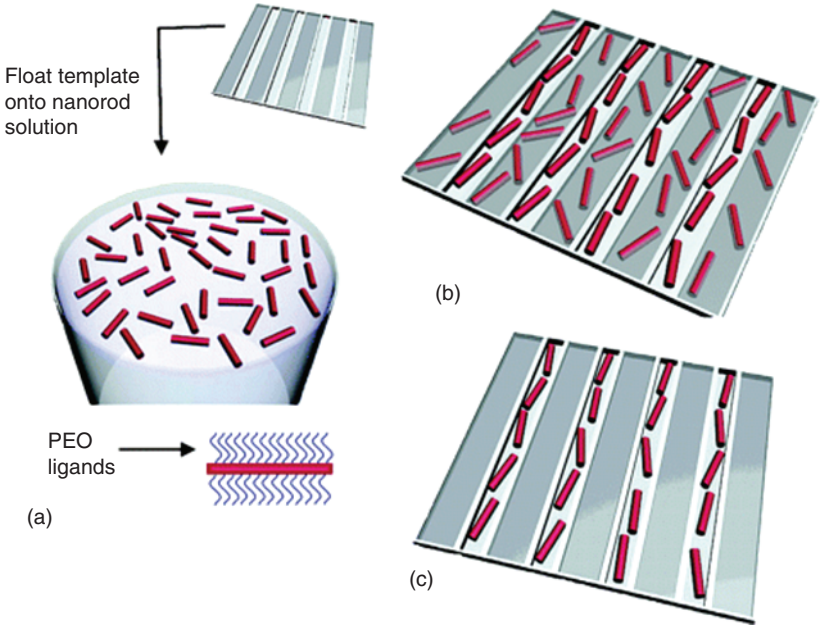

Figure 1.3 Scheme of assembling CdSe NRs using a patterned template generated by phase separation of BCPs on the substrate. (a) Floating template on an aqueous solution of PEO-capped CdSe NRs. (b) PEO-capped CdSe NRs within the channels and on the surface of PS template. (c) CdSe NRs isolated in channels after rinsing the template. (Zhang *et al*. 2006 [23]. Reproduced with permission of American Chemical Society.)

For instance, Thorkelsson *et al.* accomplished the end-to-end alignment of CdS NRs into large-area structures in PS-*b*-P4VP films using the solvent annealing method [25]. Vaia *et al*. demonstrated the control over single- and double-column arrangement of Au NRs with orientation parallel and perpendicular to template strips of poly-2-vinylpyridine (P2VP) regions on a substrate [26].

In addition to templates with defined shapes, fluid-like assemblies of liquid crystals can be used to guide the assembly of 1D NCs. Liquid crystal molecules are known to assemble into a range of liquid-crystalline phases such as nematic, smectic, chiral nematic or cholesteric, and cubic blue phase. These phases can serve as "soft" scaffolds to organize NRs into long-range-ordered structures [27, 28]. For example, Smalyukh and coworkers demonstrated the self-alignment of Au NRs in the anisotropic fluids of liquid crystals [29]. Nematic and hexagonal liquid-crystalline phases of a tertiary mixture composed of benzyl alcohol, CTAB, and water were used to guide the alignment of Au NRs along the liquid crystal director. When a magnetic field or shearing force was applied, the orientation of Au NRs could be switched, owing to the realignment of liquid crystals under external field. This method allows the unidirectional alignment of NRs in the liquid crystal matrix over large areas (up to millimeters), thus facilitating their applications as bulk optical metamaterials. Defects in the liquid-crystalline superstructures can be also used to assemble NCs; for example, the topological defect cores within the self-organized blue phase of 3D cubic nanostructures can provide natural templates to trap colloidal NCs [30]. However, to date only a few types of NPs have been assembled by using these 3D topological templates [31].

Compared to geometrically patterned templates, chemical patterns afford additional flexibility in guiding the assembly of NCs due to the selectivity in interactions between NCs and the templates. Thus, this method enables the control of the spacing and orientation of NCs. However, assembly using chemical patterns heavily relies on the chemical interactions between the particles and the templates. As a result, this method usually requires surface modification of NCs and molecular design of templates, and mostly these templates cannot be repeatedly used.

1.2.2 Field-Driven Assembly

The intrinsic shape anisotropy of 1D NCs makes it possible for them to be readily aligned under an external field (e.g., electric, magnetic field, or fluidic shearing). The literature is replete with research on the directed assembly of NCs under external fields. In this section we review several types of field-driven assembly strategies, including electric- or magnetic-field-assisted assembly as well as assembly in fluid flows.

1.2.2.1 Assembly under Electric Field

Electric field is an ideal external stimulus to drive the organization of 1D NCs that carry a net charge or permanent induced electric dipole moment. Under an electric field, NCs with a net charge align their longitudinal axis along the direction of the field lines and migrate toward the electrode of the applied electric field. When there is no net charge, the polarization of NCs under electric field

induces the dipole–dipole interaction between NCs, which drives the alignment of NCs parallel to the field lines. The dipole–dipole interactions between particles are denoted as $U = \pi\varepsilon_0\varepsilon_s|C|^2a^3E^2$, where ε_0 is the permittivity of free space, ε_s is the solvent dielectric constant, C is the dipole coefficient, a is the particle radius, and E is the field amplitude [32]. For 1D NCs, the potential energy of orientation is related to the anisotropy in electric polarizability of NCs, which is determined by the electric polarizabilities parallel and perpendicular to the main axis of the NCs [33]. The key challenge in arraying NCs from chaotic dispersion is to make the dipole–dipole interaction strong enough to overcome the thermal energy kT. To assemble NCs by this method, electrodes are placed parallel or perpendicular to the substrate to apply a direct current (DC) or alternating current (AC) electric field. To ensure the orientation of NCs, a number of parameters need to be tuned, including the magnitude of electric field, frequency of the alternating voltage, size of NCs, ligand on NCs, and the solvent [32, 34].

Semiconducting CdS and CdSe NRs possess induced and/or permanent dipole moment due to their noncentrosymmetric wurtzite lattice. When an external electric field is applied, these NRs preferentially align along the direction of field lines. Drndic *et al*. demonstrated that trioctylphosphine oxide (TOPO)-capped CdSe and CdTe NRs align along the direction of applied electric field and accumulate within the nanoscale gaps of the electrodes. NRs dispersed in a hexane/octane solution were drop-cast on to a device patterned with electrode pairs. After the application of a voltage to the electrodes, the majority of NRs oriented parallel to the electric field inside the gap of the electrodes [35]. A study on the relationship between the polarizability and the size of TOPO-covered CdSe NRs in cyclohexane under electric field confirmed the existence of permanent dipoles as well as the correlation between the dipole strength and volume of NRs [36]. The unscreened permanent dipole moments of the NRs were found to linearly increase with increasing volume. Golan *et al*. reported a direction-switchable assembly of elongated microstrings of hexadecylamine-capped CdS NWs or thiol-capped CdS NRs in toluene under an electric field. The head-to-tail connection of NRs was associated with the *c*-axis of the wurtzite structures orienting along the major axis of NRs/NWs and eventually the axis of the microstrings [37].

When an electric field is combined with slow solvent evaporation, the assembly process produces structures with closely packed NRs. For instance, upon the evaporation of toluene, CdS NRs aligned perpendicular to the substrate to form 2D hexagonal arrays under a DC electric field [38]. Additionally, the assembly process produced an AB-layered 3D superlattice of NR arrays in which the upper NRs were selectively placed in the interstitial spacing between NRs in the underlying layer. Russell and coworkers reported the assembly of densely packed hexagonal arrays of CdSe NRs perpendicular to the underlying substrate by slow evaporation of alkane-functionalized CdSe NRs in a polymer matrix under an electric field (Figure 1.4) [40]. As shown in Figure 1.4a, a mixture of PMMA and CdSe NRs covered with tetradecylphosphonic acid and TOPO in chloroform was placed on a silicon wafer, and an electric field was applied during the slow evaporation of solvent. During solvent evaporation, CdSe NRs segregated from the PMMA matrix and corralled into arrays with a hexagonal close-packed arrangement of NRs (Figure 1.4b). When the field was removed, the NR arrays

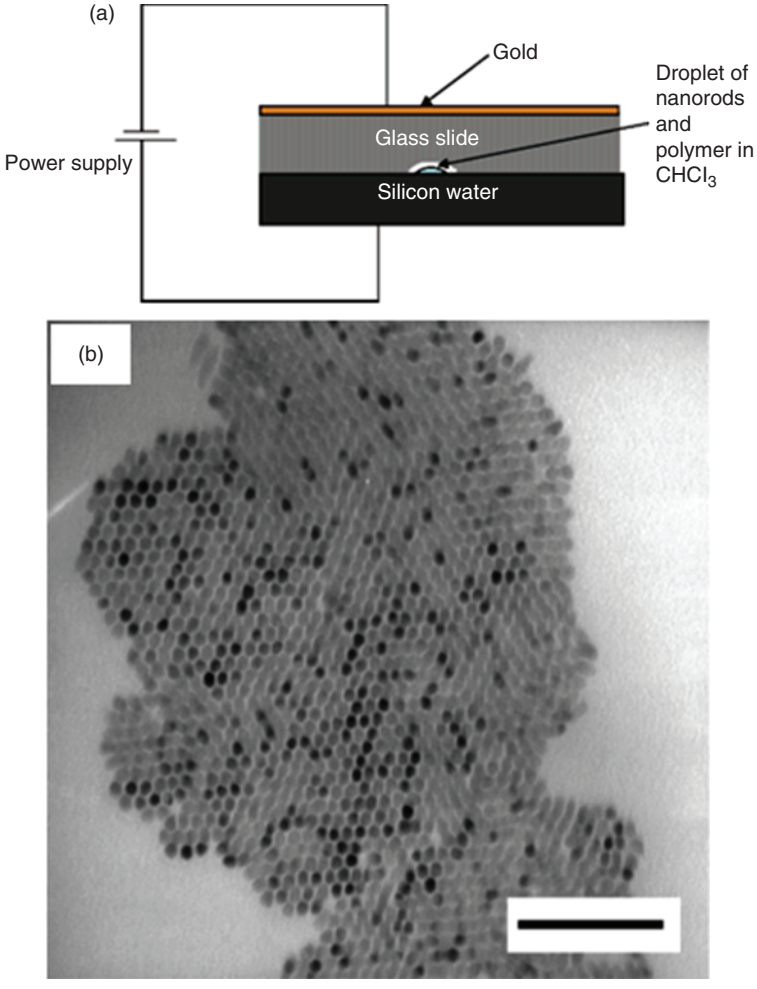

Figure 1.4 (a) Scheme of experimental setup for electric-field-assisted assembly of CdSe NRs. (b) TEM image of the "self-corralling" of CdSe NRs in PMMA. Scale bar: 100 nm. (Huang *et al*. 2016 [39].Reproduced with permission American Chemical Society.)

were retained within the thin NR/polymer composite film. It was found that the strong, unfavorable polymer–ligand interaction was essential to the formation of densely packed arrays.

The polarizability of NCs is crucial to the orientation and organization of NCs under an electric field. For a 1D structure with low polarizability (e.g., silicon NWs), a higher strength of electric field is required to achieve the assembly and alignment of NWs [41]. The shape anisotropy of 1D NCs also influences their ordering behavior under an electric field. One interesting example is the chaining of polystyrene colloidal ellipsoids aligned and titled in an angle with respect to the direction of the applied field, where the angle is strongly dependent on the aspect ratio of the ellipsoids [42]. Moreover, when additional confinement

is introduced to assist the assembly, more complex structures can be obtained. For instance, Zhu *et al*. recently reported the electric-field-driven assembly of polystyrene-tethered Au NRs in anodic aluminum oxide (AAO) channels [43]. Within the confined space, the external electric field could initiate the rotation of Au NRs and keep their orientation along the axis of electric field. By varying the inner diameter of the AAO channel, length of ligands on NRs, and orientation of electric field, various hybrid assemblies were generated, including single to quadruple helix as well as linear and hexagonally packed structures of NRs.

1.2.2.2 Magnetic Field

Magnetic field has been widely used for organizing 1D NCs with permanent or field-induced magnetic dipole moment. Magnetic field can be generated by permanent magnets or electromagnets. The magnitude and spatial distribution of the field can be tuned by changing the position of magnet relative to the building blocks. Under an external magnetic field, the dipole–dipole interactions between particles can be attractive or repulsive depending on the angle between the magnetic field and the line connecting the dipoles of the particles [44]. For 1D NRs, the dipole–dipole interactions between NRs are attractive when the NRs take the head-to-end configuration, while it is repulsive for the side-by-side configuration. The dipole moment of NRs gets aligned along the magnetic field line to form chains when the dipole–dipole interaction is at least one order of magnitude greater than thermal energy. For instance, nickel NWs formed chains in the head-to-tail configuration in a low-viscosity solvent when a low magnetic field was applied. When the viscosity of liquid was increased, the NWs aligned parallel to the field in response to the magnetic torque [45]. The attractive force (f) between two NWs of lengths L_1 and L_2 can be approximated as

$$f = -Q_m^2 \left(\frac{1}{r^2} - \frac{1}{(r+L_1)^2} - \frac{1}{(r+L_2)^2} + \frac{1}{(r+L_1+L_2)^2} \right)$$

where Q_m is the magnetic field of one NC, and r is the end-to-end NC separation. This theoretical model is based on the assumption that the magnetic dipole–dipole forces and viscous drag are dominant. It suggests that the chaining of NWs is due to the combined effect of the dominant magnetic forces and the viscous drag of the solvent.

When the concentration of NRs increases, the individual chains may become unstable, leading to the formation of 2D arrays of NRs. For example, solvent evaporation of a diluted dispersion of FePt NRs in hexane on silicon wafer between two magnets led to the formation of 2D hexagonal mesophase assemblies with side-by-side arrangement of NRs [46]. In another work, millimeter-sized assemblies of aligned cobalt NRs were obtained by drying a dispersion of the NRs under a homogenous magnetic field [47]. When the concentration of NCs is high, 3D structures can be obtained. As an example, 3D triclinic crystal structures were produced by assembling ellipsoidal Fe_2O_3/SiO_2 core–shell particles under a magnetic field [48]. The assembly was performed by vertically placing a glass slab into a suspension of magnetic ellipsoids, above which a magnet was placed to generate a static magnetic field. During the drying process,

the capillary force drove the particles to closely pack, while the magnetic force facilitated the directional organization of the particles.

Shape and constituent anisotropy of NCs can be introduced to control the assembly pathway to produce new assembled structures. Granick *et al*. developed a magnetic-field-assisted assembly of magnetic Janus rods into a fascinating class of colloidal ribbons and rings [49]. Silica rods were coated with a hemicylindrical nickel layer to provide permanent dipole and anisotropic interactions. When the Janus rods were subjected to a strong magnetic field, individual rods aligned their short axis along the magnetic field and stacked into ribbons (Figure 1.5a). A close inspection of the assemblies shows three types of deformation on the ribbons: bend, splay, and twist (Figure 1.5b), when the energetic cost was gradually increased. The rods in the ribbons lined up in two different ways: a trans configuration where rods alternately faced each other in a zig-zag chain, and a cis configuration in which the magnetic sides of two adjacent rods faced the same direction (Figure 1.5c). When the field direction was switched, the ribbons bucked into rings due to the faster response of the ends of the ribbon to follow the reversed field than the main body of ribbon. Figure 1.5d shows three cyclic structures of the same ribbon obtained from repeatedly reversing the field. The curving of ribbon-ends in the same direction resulted in a completed loop (Figure 1.5d-1), while the curving of ribbon-ends in opposite directions led to an S-shaped intermediate structures that transiently

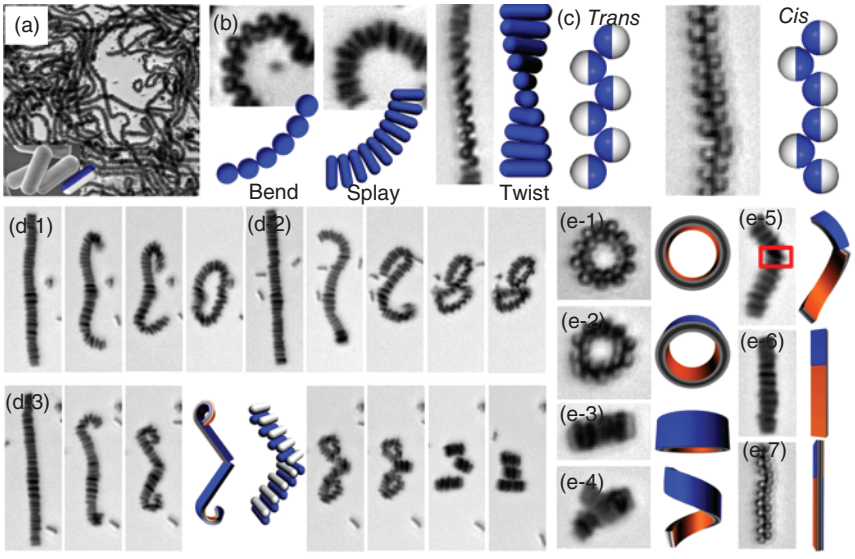

Figure 1.5 (a) SEM image of ribbons of magnetic Janus rods. Scale bar, 5 μm. (b) Deformation modes of ribbon: images accompanied by schematic illustrations. Scale bar: 2 μm. (c) End-on view of a ribbon accompanied by schematic illustrations. Scale bar: 2 μm. (d-1) Single ring forms from linear ribbon through a C-shaped intermediate. (d-2) Two ring forms from a linear ribbon through the S-shaped intermediate. (d-3) Three rings formed from a linear ribbon. Scale bar: 4 μm. (e-1–e-7) Deformation of ring to form a ribbon in response to a small field. Scale bar: 2 μm. (Yan *et al*. 2013 [49]. Reproduced with permission of Nature Publishing Group.)

collapsed into the shape of "8" and subsequently split in the middle to form two separate rings (Figure 1.5d-2). When the direction of magnetic field was reversed rapidly, the ribbon suddenly developed into a singularity and finally broke into three small individual rings (Figure 1.5d-3). Moreover, when a low magnetic field was applied, the rings broke into ribbons that aligned with the field through a pathway shown in Figure 1.5e. This work demonstrates the fascinating complexity that can be achieved in a nonequilibrium dynamic assembly system.

1.2.2.3 Flow Field

As a universal directional force, flow field can be used to direct the assembly of NCs, not restricted to NCs with electric or magnetic dipole. The shearing force imposed by the flow can drive the NCs to align in the direction of the flow, similar to the flow of a river pushing logs parallel to the riverside. Microfluidic technique is often adopted for the assembly of NCs, in combination with confinement of selectively patterned surface. When a suspension of 1D NCs passes through a microfluidic channel, the NCs preferentially aligned along the flow direction due to the shear force. The alignment and organization of NCs will be destroyed when the flow field is removed. Thus, a chemically patterned surface is used to preserve the assembled structures through the chemical interactions between NCs and the substrate. A pioneering work by Lieber *et al*. showed that parallel arrays of NWs with controllable separation and a complex crossed NW array can be fabricated by using fluidic channels [50, 51]. The scheme in Figure 1.6 illustrates the assembly process while the NW suspension flows inside a PDMS-based microfluidic channel. A variety of NWs with different dimensions and compositions (e.g., gallium phosphide, indium phosphide, and silicon NWs) were used as building blocks in this work. With controlled flow rate and duration, parallel arrays of NWs with up to millimeter length scales were fabricated. The degree of alignment could be improved by increasing the flow rate. The average separation of the aligned NWs was negatively correlated with the flow duration. Moreover, crossed and more complex structures could be realized by sequentially assembling NW arrays with different flow directions in a layer-by-layer manner [52, 53].

The assembly of NCs can be triggered by varying the solvent composition of fluids when the surface of NCs is functionalized with ligands that are responsive to the quality of the solvent. For instance, Nie and coworkers used a microfluidic flow-focusing device to assemble amphiphilic BCP-tethered Au NRs into Janus-like vesicles that could act as vesicular motors for controlled release [54]. In this work, PEO-*b*-PS-tethered Au NRs dispersed in tetrahydrofuran were introduced into the central channel, while two steams of water were introduced from two side channels. Water works as a poor solvent for the PS blocks of BCP tethers. The diffusive mixing of the two fluidic flows along the transverse direction changed the quality of the solvents and triggered the formation of hybrid vesicles. The diameter and phase domains of Janus vesicles are dependent on the flow rates of fluids and the relative concentration of the building blocks.

As mentioned previously, the field-driven assembly shows the following advantages over the others: First, it allows effective control over the directionality of NC arrays by varying the field direction. Second, the driving forces of assembly can be readily tuned by controlling the direction, magnitude, and spatial distribution

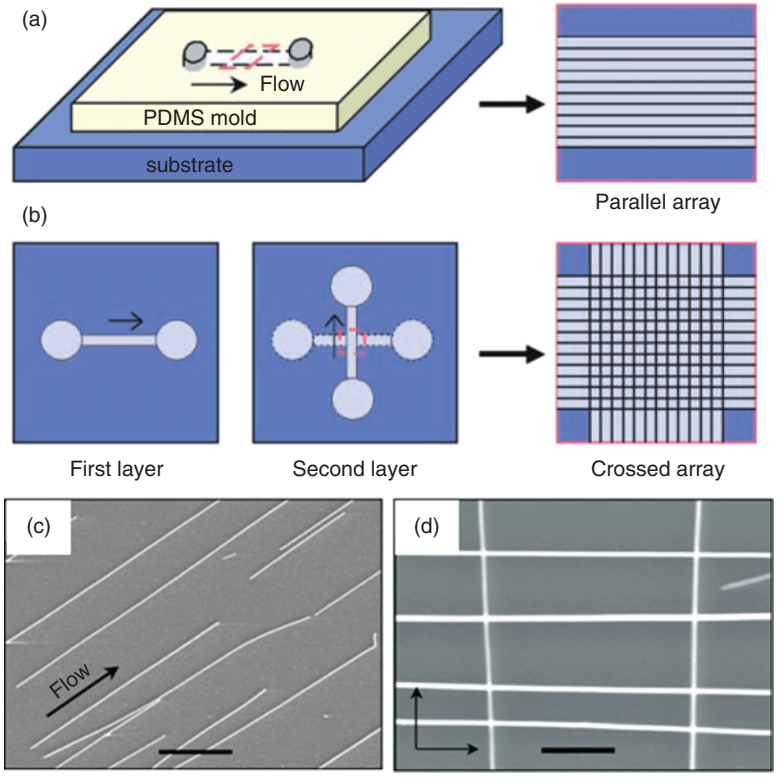

Figure 1.6 (a,b) Scheme of flow assembly to form (a) a parallel NW array and (b) a multiple crossed NWs array using fluidic channel. (c) SEM image of parallel arrays of indium phosphide NWs. (d) SEM image of crossed arrays of indium phosphide NW. Scale bar: 2 μm. (Liu *et al*. 2012 [51]. Reproduced with permission of American Chemical Society.)

of the field. As a result, the field-driven assembly can be designed to be reversible and switchable. Third, when an electric or magnetic field is used, the assembly process is independent of the experimental conditions such as pH, temperature, and solvent quality, because there is no direct contact between NCs and source of the field. Last but not least, it is scalable and can be used for the fabrication of large-area assembled structures. This assembly method, however, has some limitations. Electric- or magnetic-field-assisted assembly requires that the NCs be responsive to the field. Additional treatment of the resulting assemblies is required to retain the structures after the field is removed. Moreover, as most fields is one dimensional, the diversity of the assembled structures is limited.

1.2.3 Assembly at Interfaces and Surface

Interfacial assembly has been widely explored for assembling NCs into 2D periodical arrays or 3D lattice structures. The organization of NCs is driven by the reduction in the interfacial energy when particles are transferred from one phase to the interface. Depending on the types of interface, the assembly method can be classified into several categories, such as liquid–liquid, liquid–air, and

liquid–solid assembly. Controlled solvent evaporation is commonly used to confine the particles within a predetermined area.

1.2.3.1 Liquid–Liquid Interface

The self-assembly of particles at a liquid–liquid interface started a century ago when Pickering and Ramsden observed that micro-sized particles (e.g., silica particles) formed a resistant film at the interface, which is called the Pickering emulsion [55, 56]. Later Pieranski pointed out that the assembly of spherical particles at the oil/water interface is due to the decrease in the total free energy by the placement of a particle at the interface. The reduction in energy can be described using the following equation [57]:

$$\Delta E = -\frac{\pi r^2}{\gamma_{O/W}} \cdot [\gamma_{O/W} - (\gamma_{P/W} - \gamma_{P/O})]^2$$

Here, r is the radius of the particle, and $\gamma_{O/W}$, $\gamma_{P/W}$, and $\gamma_{P/O}$ are the interfacial tension between oil/water, particle/water, and particle/oil, respectively. For rod-like particles, the interfacial energy change by placing an NR onto the interface can be divided into $\Delta E_{//}$ and $\Delta E_{\perp}$, which correspond to the orientation of a single NR parallel or perpendicular to the interface, as given by [58–60]

$$\Delta E_{//} = 2\pi RL[\pi(\gamma_{P/O} - \gamma_{P/W}) + \theta(\gamma_{P/W} - \gamma_{P/O}) + \gamma_{O/W} \sin\theta]$$

where

$$\cos\theta = \frac{\gamma_{P/W} - \gamma_{P/O}}{\gamma_{O/W}} \quad (L \gg R)$$

$$\Delta E_{\perp} = \pi R^2(\gamma_{P/W} - \gamma_{O/W} - \gamma_{P/O}) + 2\pi Rh(\gamma_{P/W} - \gamma_{P/O})$$

In the above equation, the size of NRs is defined by the radius R and length L; the contact angle of the NR at the interface is represented by θ; and h is the penetration depth of NR into the water phase when it is perpendicular to the interface. Russell and Emrick *et al*. studied the assembly of TOPO-covered CdSe NRs at the toluene/water interface and found that the NRs preferred to orient parallel to the plane of interface at low concentration. This was attributed to the fact that the interfacial energy loss $\Delta E_{//}$ is about 40 times larger than $\Delta E_{\perp}$, which is due to the larger surface area for parallel orientation of NRs compared with perpendicular orientation [46]. The assembly process is dependent on a number of parameters, including size and concentration of NR, the wettability of particle surface, and the choice of the two liquids. The large area of smectic/nematic structures of laterally aligned NRs can be obtained by solvent evaporation from a suspension of NRs in a volatile solvent on top of water [61, 62].

NWs with aspect ratio much larger than NRs are more favorable to adopt a parallel orientation at the interface. For instance, a millimeter-sized monolayer of densely aligned Au NWs was obtained by spreading oleylamine-coated Au NWs dispersed in hexane on diethyleneglycol (DEG) [63]. The long-range ordering of NW arrays can be used to guide the lateral assembly of other small building blocks such as nanospheres (NSs) and NRs in a binary assembly system. For instance, Liz-Marzán and coworkers reported the binary self-assembly of Au NWs and Au NSs/NRs at a liquid–liquid interface [64]. A mixture of Au NWs and Au NSs/NRs

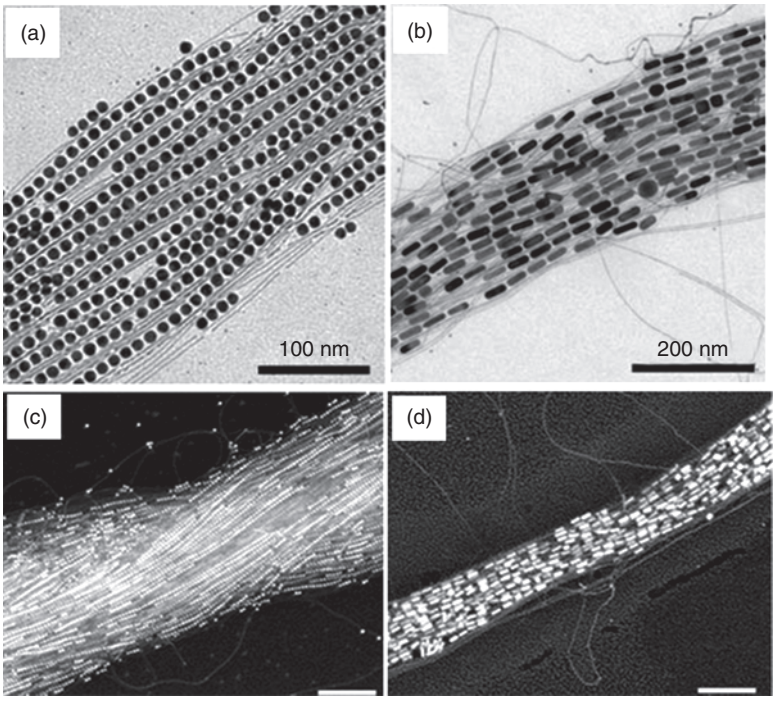

Figure 1.7 (a,b) TEM images of linear binary assemblies of (a) Au NS and (b) Au NRs with Au NWs. (c,d) SEM images of (c) Au NSs and (d) Au NRs embedded in Au NW bundles. Scale bar: 200 nm. (Sánchez-Iglesias *et al*. 2010 [64]. Reproduced with permission of John Wiley & Sons.)

was dispersed in hexane and drop-cast on the surface of DEG. The evaporation of hexane in a controlled manner led to the formation of a film of binary assemblies in which the NWs acted as an oriented template to guide the linear organization of NPs or NRs along the long axis of the NWs (Figure 1.7a,b). In contrast, drying of the same colloidal mixture on a solid substrate led to the formation of 3D NW bundles integrated with NSs and NRs (Figure 1.7c,d).

The template of liquid–liquid interface can arise from the condensation of water droplets during the fast evaporation of volatile solvents. Khanal and Zubarev used condensed water droplets to template the organization of Au NRs into ring-like superstructures [65]. Upon evaporation of the solvent, PS-coated Au NRs dispersed in dichloromethane (CH_2Cl_2) spontaneously assembled into ring structures with high yield. The ring formation was attributed to the template effect of the water droplet/CH_2Cl_2 interface formed from the condensation of water during the evaporation of the highly volatile solvent.

1.2.3.2 Liquid–Air Interface

The assembly of 1D NCs at the liquid–air interface via the Langmuir–Blodgett (LB) technique can produce a large-area monolayer of parallel NCs. As shown in Figure 1.8, NCs dispersed in a volatile organic solvent (e.g., chloroform or hexane) are spread evenly over a water surface using an LB trough. The NCs form a water-supported monolayer at the interface after the evaporation of

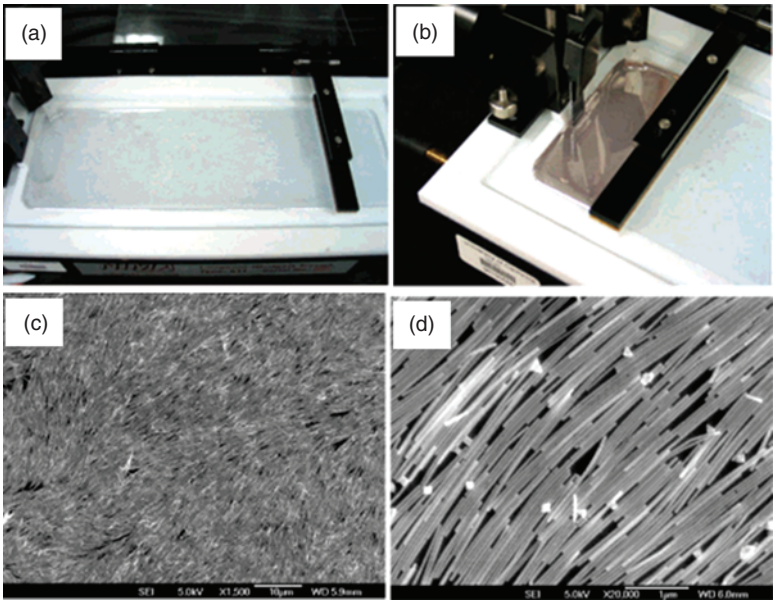

Figure 1.8 (a,b) LB NW assembly process at the (a) initial and (b) final compression stage. (c,d) SEM images of Ag NWs monolayer at different magnifications. (Tao *et al*. 2003 [66]. Reproduced with American Chemical Society.)

the top liquid. Lateral compression at a controlled speed generated a compact monolayer of ordered NC arrays, which could be subsequently transferred to desired substrate by horizontal or vertical lift-off. Large-scale assemblies of both closely packed arrays and well-defined patterns with low packing density of 1D NCs have been produced by using the LB technique [66–69]. The formation of NC arrays can be tuned by varying the size, passivating ligand of NCs, and surface pressure. A pioneering work by Yang and coworkers reported the fabrication of a monolayer of Ag NW arrays with area over 20 cm^2 using this technique [66]. Ag NWs were functionalized with 1-hexadecanethiol ligands to render a hydrophobic surface and were dispersed in chloroform. The packing density of NWs increased gradually with the increase of surface tension. Above a certain value of the surface tension, the monolayer underwent an insulator-to-metal transition, implying a remarkable side-by-side alignment of Ag NWs parallel to the trough barrier (Figure 1.8c,d). Owing to the ease in transferring the assembled film to a desired substrate, multilayer films can be prepared by repeatedly depositing monolayer film onto the substrate to produce mesh-like mesostructures with a defined cross-angle between layers in a layer-by-layer manner [69–71]. For instance, Yu *et al*. packed two layers of Te NWs into nanoscale mesh-like assemblies with different cross-angles between NWs in different layers [71]. It is worth mentioning that, in order to disperse NCs in solvents above the water phase, it is usually necessary to functionalize them with a hydrophobic capping agent via ligand exchange.

When relatively short NRs are used, the organization of NRs is largely dependent on the size, aspect ratio, and surface functionality of the NRs [67, 72, 73]. In a study by Yang *et al*., $BaCrO_4$ NRs with small aspect ratios (3–5.1) exhibited an assembly transition from isolated raft-like aggregates to 2D smectic arrangement and further to 3D nematic configuration with increasing surface pressure [72]. In contrast, longer NRs with an aspect ratio of ~150 assembled into a nematic layer with NRs aligned roughly along the same direction and into bundles of NRs when the compression was strong. This experimental observation is in good agreement with simulations results on the phase behavior of hard rods.

1.2.3.3 Evaporation-Mediated Assembly on Solid Surface

Evaporation-mediated assembly offers a simple, inexpensive method to produce highly ordered, close-packed superstructures of 1D NCs on a solid surface. Typically, a dispersion of NCs is allowed to dry and assemble on the solid substrate into well-ordered structures under a confined geometry and at a controlled drying rate. During the drying process, if the evaporation of liquid is faster than the diffusion of NCs in liquid, the local particle concentration will be larger in the area right underneath the liquid surface. Surface tension will drive the self-assembly of NCs into a 2D monolayer at the surface. Continuous evaporation results in the formation of another layer on the surface of the first layer. The receding of the evaporation front pulls the particles in solution toward the drying front by convection, depositing well-ordered particles in the drying front gradually.

The organization of NCs is largely determined by several parameters including the shape and concentration of NCs, assembly conditions (e.g., solvent, temperature), and surface property (e.g., hydrophobicity) of the substrate [74]. Wang *et al*. studied the shape dependence of the assembly of Au NCs by solvent evaporation [75]. Au NRs assembled preferentially into nematic or smetic A phase, while other shaped NCs such as polyhedra, nanocubes, and bipyramids formed hexagonally packed, tetragonally packed, and nematic ordered 3D structures, respectively. When binary Au NRs with different diameters (and different resulting aspect ratios) are used, the two populations of NRs self-separated to form smectic superstructures. Korgel *et al*. explored the self-assembly of CdS NRs at a relatively low surface coverage on a substrate. The assembly process produced networks of stripes consisting of NRs packed next to each other and aligned parallel to the stripe direction, rather than close-packed assemblies. Increasing the concentration of NRs led to the formation of perpendicular orientation of NRs in a smectic phase [76].

The evaporation rate of the solvent, which is dependent on factors such as temperature, partial pressure, and volatility of solvents, is crucial to the formation of well-ordered structures. In addition, a few other parameters such as polarity and permittivity (for charged ligand) of the solvent also play an important role in controlling the solubility and interaction of NCs. As an example, Koster *et al.* observed the transition of NR assemblies from nematic to hexagonal packing when the solvent was changed from nonpolar (e.g., toluene) to polar (e.g., ethanol or water) [77].

The aforementioned study illustrates the inherent complexity in the dynamical process of drying-mediated self-assembly [78, 79]. To better understand and control the assembly, it is necessary to systematically optimize the assembly conditions and quantitatively assess the assembled structures. For instance, Alivisatos *et al*. aligned CdS NRs vertically on many device-relevant substrates at the centimeter scale and quantitatively analyzed the orientation distribution of NRs over the entire film [79]. The assembly was triggered by drying octadecylphosphonic acid (ODPA)-covered CdS NRs in hexane in a controlled manner. Grazing-incidence wide-angle X-ray diffraction was used to characterize the assembly morphology and orientation of NRs. The quantitative study established a correlation between the assembly conditions (i.e., temperature, aspect ratio of NRs, and substrate) and the overall orientation of NRs. At the optimal condition, 96% vertical alignment of NRs on 1 cm^2 silicon nitride substrate was obtained (Figure 1.9).

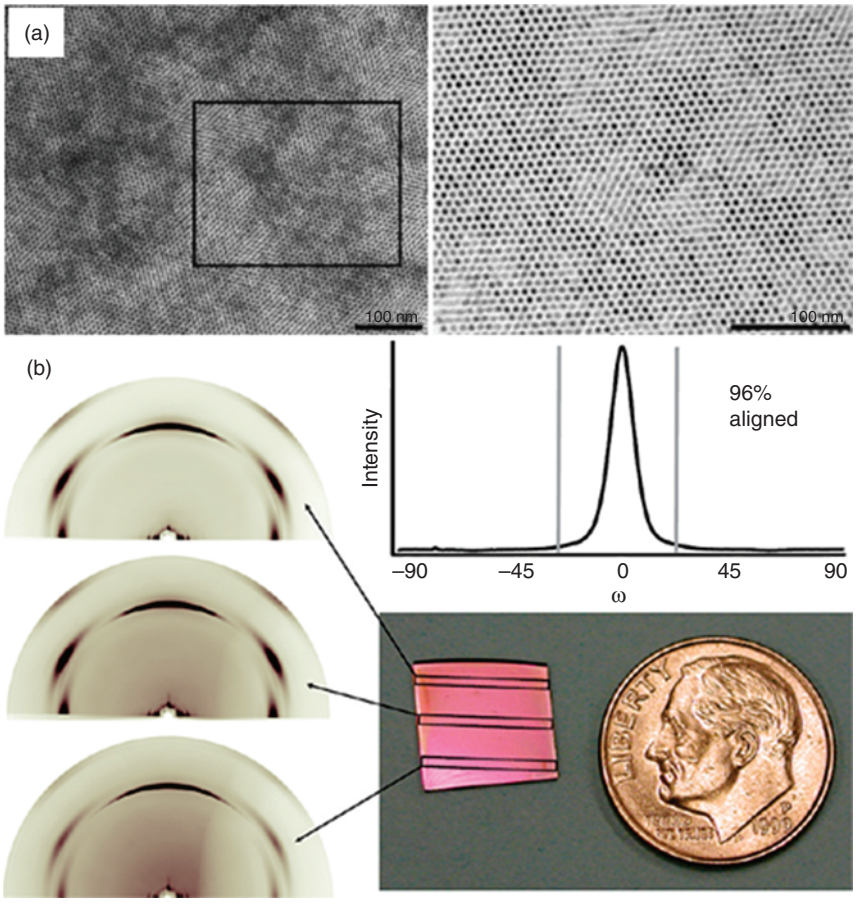

Figure 1.9 (a) SEM mages of vertically oriented CdS NRs with progressive zoom from left to right. (b) Ninety-six percent vertical alignment of CdS NRs on a device scale (1 cm^2). (Baker *et al*. 2009 [79]. Reproduced with permission of American Chemical Society.)

Self-assembly at the interface and surface provides a facile and affordable way to efficiently organize 1D NCs into ordered large-area structures. The assembly method does not require expensive apparatus. A rich variety of assembly morphologies can be obtained, including loose or close packing, parallel or vertical array, and monolayer or multilayer of 1D NCs. In this method, solvent and ligands on the NCs have to be carefully selected and assembly conditions optimized before ordered large-area structures can be generated. However, the complexity and hierarchy level of the overall assemblies by this method are restrained by the nature of this method. In order to achieve more complex organization of NCs, it is usually necessary to combine this approach with other assembly techniques.

1.2.4 Ligand-Guided Assembly

Functional ligands capped on the surface of NCs or dispersed in solution are routinely employed by chemists to control the organization of NCs at the molecular level. Generally, a diverse range of ligands (e.g., small molecules, polymeric species, or biomolecules) can contribute to the assembly of NCs in the following ways: (i) as a linker to guide the assembly via molecular recognition of functional groups; (ii) as a scaffold to direct the assembly via both spatial and chemical template; and (iii) as depletant additives to drive the assembly via depletion force. As a result, this assembly strategy allows the organization of NCs into structures with high complexity or precision.

1.2.4.1 Small Molecules

In general, small molecules possessing short chains diffuse faster and bind more efficiently to the surface of NCs than large molecules. Small molecules have been extensively explored for guiding the assembly of 1D NCs. A frequent choice of such ligands is bifunctional molecules in which one group binds to the NCs and leaves the other group free to bind another NC. Bifunctional ligands such as dithiol molecule, thioalky carboxylic acids, cysteine, and glutathione can be used to drive the end-to-end assembly of Au NRs due to the preferential attachment of these capping agents to the ends of NRs [80–83]. For instance, Thomas *et al*. reported the end-to-end assembly of Au NRs into chains in the presence of α,ω-alkanedithiols [80]. The length of the NR chains was dependent on the concentration of α,ω-alkanedithiols, suggesting a chaining mechanism involving the dimerization and subsequent oligomerization of NRs. Other than covalent or hydrogen bonds of bifunctional linker, a series of molecular interactions can be employed to guide the assembly of 1D NRs or NWs in an end-to-end and/or side-by-side manner. They include solvent-mediated hydrophobic interactions between alkanethiol [84], coordination bond formation of transition-metal complexes [85], and electrostatic interactions between charged NCs (or between charged linkers and NCs) [86]. Recently, thiol-containing alkynylplatinum(II) terpyridine complexes were used to direct the end-to-end connection of Au NRs through the formation of Pt· · ·Pt and π–π stacking interactions [87].

The addition of a nonsolvent ligand, (i.e., depletant additive) can induce instability and subsequent assembly of NRs [88–90]. Cao and coworkers reported

the assembly of CdSe/CdS core–shell semiconducting NRs into spherical or needle-shaped superparticles with multiple supercrystalline domains by overcoating the NRs with the surfactant dodecyltrimethylammonium bromide (DTAB) [88, 91]. As shown in Figure 1.10, CdSe/CdS NRs originally capped with octylamine and ODPA were first transferred to water to form an NR-micelle solution by mixing the NRs with an aqueous solution of DTAB. Subsequently, continuous transfer of the NR-micelle solution into ethylene glycol led to the detachment of the DTAB molecule from the NRs and triggered the fast assembly of NRs. The amount of DTAB was found to affect the kinetics of superparticle formation and control the size of the superparticles. The selective removal of ligand of NRs can also change the surface chemistry and drive the anisotropic interactions among NRs [92, 93]. Recently, an end-to-end connection of CdSe NRs driven by the ligand desorption–adsorption equilibrium at the NR surface was reported by Nakashima *et al*. CdSe NRs were modified with water-soluble small-molecule thiols such as 2-(dimethylamino)ethanethiol hydrochloride (DMAET). During static aging of the aqueous solution, the weaker binding affinity of DMAET at the NR ends led to the formation of

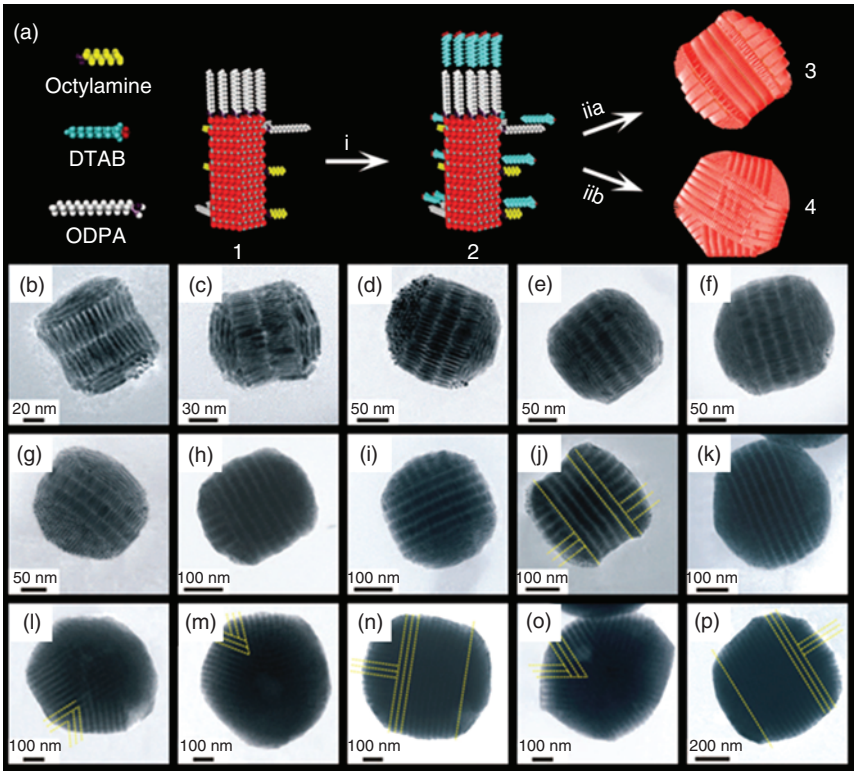

Figure 1.10 (a) Schematic illustration of the formation of superparticles form CdSe/CdS NRs. (b–p) TEM images of superparticles made from NRs of length 28 nm and width 6.7 nm. (Abécassis 2016 [91]. Reproduced with permission of John Wiley & Sons.)

amphiphilic NRs with hydrophobic ends and hydrophilic sides and to the consequent end-to-end association of such NRs due to hydrophobic effect [92].

The above-mentioned small molecules spontaneously interact to drive the assembly upon NC collision. In addition, molecular linkers that can be regulated by external stimuli such as light and pH change are also attractive for the development of responsive assembly systems [83, 94, 95]. Liz-Marzán *et al*. reported the use of femtosecond laser irradiation to assist the assembly of Au NRs into dimers while inhibiting the formation of trimers and longer oligomers [95]. In their work, dithiol was used as molecular linker. Au NRs with the appropriate aspect ratio were used to ensure that the laser wavelength was in resonance with the longitudinal LSPR bands of trimers and longer oligomers but above that of monomers and dimers. Upon irradiation at 800 nm, the localized enhancement of the electromagnetic field at the interparticle gap led to an increase in local temperature and decomposition of molecular linkers within trimers and longer oligomers, thus leading to a significant increase in the yield of dimers. The pH dependence of ligands provides another route to achieving real-time control over the assembly of NRs. For example, Wang *et al*. reported a reversible, pH-controlled assembly of Au NRs by mixing NRs with a class of bifunctional molecules such as 3-mercaptopropionic acid, 11-mercaptoundecanic acid, glutathione, and cysteine [83]. The different charge states of these molecules in selective pH ranges were assumed to result in the reduction of the local repulsion between NRs and hence in the assembly of NRs.

1.2.4.2 Polymeric Species

Polymers represent an attractive class of ligands for guiding the assembly of NCs, as the functionality of polymers can be readily tailored for different applications [3, 96, 97]. According to Glotzer's simulation studies, amphiphiles made from polymer-tethered NCs can be considered as a new class of "macromolecules" whose assembly can be controlled for the generation of new materials [98, 99]. These building blocks have the features of common BCPs, while showing much richer assembly structures due to the additional features induced by the NCs' rigidity and geometry, combined with the immiscibility of the tether and the nanoparticle. Taking NRs as an example, amphiphiles consisting of NRs tethered with a single polymer at one end can form a rich variety of phases, including smectic C phase, zig-zag lamellar phase, cubic micelle phase, monolayer/bilayer arrowhead phase, tetragonally/hexagonally perforated lamellar phase, honeycomb phase, double gyroid phase, and hexagonal chiral cylindrical phase [98, 100–103]. The formation of different phases is strongly dependent on the relative fraction of the polymer tethers and the aspect ratio of tethered NR. For laterally tethered rods, the amphiphiles assemble into a centered rectangular stepped-ribbon phase, lamellar phase, helical scrolls, honeycomb grid, pentagonal grid, square grid, and bilayer sheet structures, depending on the length of NRs [104–106].

The concept of NP amphiphiles made from single polymer chain-grafted NRs is intriguing, but, to date, they have not been demonstrated in experiments. This is largely due to two reasons: (i) the challenge in the synthesis of such building blocks, and (ii) the mismatch in the dimension of single polymer chain and NR.

Instead, researchers selectively modified NRs with many polymer tethers at both ends to construct NP amphiphiles, which can assemble into various functional structures. As an inspiring example, Kumacheva *et al*. selectively grafted thiol-terminated hydrophobic PS to both ends of hydrophilic Au NRs covered with CTAB at the longitudinal side. The preferential grafting of polymers at ends can be explained by the deprivation of CTAB ligands at the (111) crystal facets at the ends of the rods. The resulting building blocks could assemble into a range of structures including rings, nanochains, bundles, NSs, and bundled nanochains in selective solvents, analogous to the ABA amphiphilic triblock copolymer (Figure 1.11) [107]. The formation of different assemblies was attributed to the amphiphilic feature of PS-grafted NRs that possess hydrophobic ends and a hydrophilic center. In a following work, the same group explored the assembly kinetics of the system and proposed a step-growth polymerization theory to quantitatively predict the assembly process [108–110]. On the basis of this assembly principle, Kumacheva *et al*. further studied the sequential assembly of multiple types of NRs into inorganic BCPs [111]. In this work, Au NRs and palladium NRs were first selectively functionalized with hydrophobic PS polymers at both ends. The binary NRs co-assembled into 1D random and diblock or triblock copolymer structures upon the addition of a nonsolvent for polymer tethers, following the step-growth polymerization theory. In another example, Duan *et al*. coated Au NRs with mixed hydrophilic PEO and hydrophobic PMMA polymer brush [112]. The amphiphilic build blocks could spontaneously form vesicular nanostructures owing to the phase separation of these two polymers. Moreover, the plasmonic vesicles could be disrupted through light irradiation or pH change. By replacing PMMA with polylactide, the vesicles could be

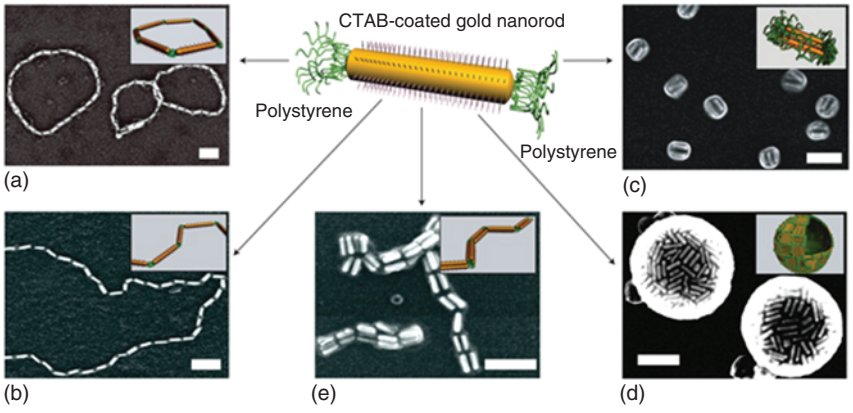

Figure 1.11 Self-assembly of polymer-tethered Au NRs in selective solvents. (a–e) SEM images of self-assembled Au NR structures: rings (a) and chains (b) formed in dimethyl formamide (DMF)/water mixture at water content of 6 and 20 wt%, respectively; side-to-side bundles of NRs (c) and NSs (d) formed on tetrahydrofuran (THF)/water mixture at 6 and 20 wt%, respectively; bundled NR chains obtained in DMF/THF/water mixture at the weight ratio of liquids 42.5 : 42.5 : 10. (Nie *et al*. 2007 [107]. Reproduced with permission of Nature Publishing Group.)

broken down by both enzymatic degradation and near-infrared photothermal heating [113].

Recently, Nie *et al*. constructed a novel type of NP amphiphiles by modifying Au NRs with linear amphiphilic BCPs [114]. These building blocks can assemble into a variety of nanostructures including micelles, disks, and vesicles in a microfluidic device. The morphology and size of the assemblies can be controlled by the flow rates of fluids in the device. More recently, Huang *et al*. used linear chains assembled from PS-grafted Au NRs and NSs as templates to synthesize multicomponent coaxial-like nanostructures via a polymer-assisted seeded-growth strategy [115]. The inner cores could be either Au NR or NSs, and the shielding layers could be Ag, Pt, Pd, or Ni metals or Cu_2O and CeO_2 metal oxides. By varying the reactant concentrations or changing the surfactants, the thickness of the shell and the shape of the overall nanostructures (Saturn-like nanostructure and coaxial-like nanostructure) could be controlled well.

1.2.4.3 Biomolecular Ligand

DNA strands are extremely attractive in precisely positioning and organizing colloidal NCs owing to their programmable base-pairing interactions, ease in introducing different functional groups, and readily automated synthesis. Single or numerous DNA strands can be bonded to the surface of NCs to guide the fabrication of discrete NC clusters or well-defined superlattices via DNA-recognition interactions [116–121]. Mirkin *et al*. studied the shape effect of NCs on their assembly behaviors using a series nonspherical NCs (Figure 1.11). They found that the shape of NCs strongly dictates the resulting crystallographic symmetry of the assembled superlattice. As shown in Figure 1.12b,c, the 2D superlattice assembled from Au NRs exhibited long-range hexagonal symmetry. Extended thermal annealing drove the reorganization of the 2D lattices into ordered 3D structures. In contrast, triangular nanoprisms, with length and width greater than its depth, assembled into 1D lamellar arrays with particles stacked in a face-to-face configuration [122]. The different packing of NCs can be explained by the directionality of the DNA interactions dictated by the particle shape. Figure 1.12a illustrates that the flat, faceted surfaces of anisotropic NCs can support the same number of oligonucleotide interactions without DNA deformation, compared to the curved surface of spherical particles. This anisotropic shape largely facilitates the directional bonding interactions by maximizing DNA linker interactions to reach the most stable structure. The complementary interactions between the DNA ligands are reversible, thus enabling responsive assembly of NCs and tunable properties of the assembled structures. For instance, the assembly and disassembly of DNA-grafted Au NRs in response to temperature variation can be used to reversibly tune the plasmonic circular dichroism response of the system [123]. Gang *et al*. fabricated 1D ladder-like ribbons with side-by-side arrangement of Au NRs using single-stranded DNA as the molecular linker [124]. The reversibility of DNA hybridization allows the temporal evolution of 1D ribbons into 3D morphology at later stages of the assembly.

Folding a programmed DNA sequence into intricate geometries constructs DNA origami, which can be used as template to program the position of NCs [125–127]. Typically, binding regions are incorporated into the origami

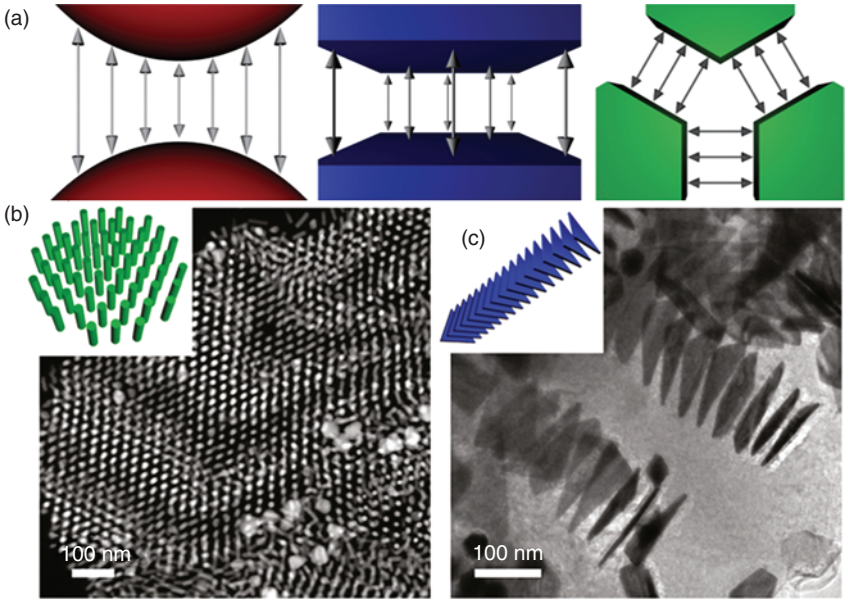

Figure 1.12 (a) Curved surface of spherical particles (left) cannot support an equal number of idealized oligonucleotide interactions without DNA deformation as flat surfaces of anisotropic nanostructures (middle and right). (b,c) TEM images of (a) hexagonal 3D layer of Au NRs and (c) 1D lamellar assemblies of Au triangular nanoprisms by DNA directed assembly. The inset shows the scheme of the NC array. (Jones *et al*. 2010 [122]. Reproduced with permission of Nature Publishing Group.)

to capture particles bearing complementary DNA sequences. Sophisticated superstructures with precisely positioned 1D NCs can be constructed by designing the pattern of the capturing strands on the scaffold [128–131]. Jiang *et al*. [132] and Du *et al*. [133] constructed a nanoplatform by assembling single Au NR on the surface of triangular DNA origami structures with DNA capture strands extended from one arm of the template. Winfree *et al*. fabricated cross-junctions of single-walled CNTs using bifacial DNA origami templates with two lines of capturing DNA strands in a cross pattern on the opposite sides of DNA origami [134]. Wang and coworkers recently produced Au NR helical superstructures with tailored chirality by using template of 2D DNA origami structures [135]. In this work, an "X" pattern of DNA capturing strands was designed on both sides of 2D DNA origami templates. Au NRs tethered with complementary DNA sequences subsequently hybridized with the DNA origami, leading to Au NR helices in which the origami intercalated between neighboring Au NRs. The handedness of Au NR helices can be altered by changing the rotation angle of the "X" pattern on the origami.

Other biological molecular recognitions (e.g., antibody–antigen interactions) have also been utilized to assemble 1D NCs. In a pioneering work by Murphy *et al*., biotin-coated Au NRs assembled end to end upon the addition of streptavidin [136]. Kotov and coworkers assembled Au NRs carrying MC-LR antibodies or its ovalbumin antigen in both side-to-side and end-to-end modes

in a controlled manner [137]. The preferential attachment of MC-LR antibodies and antigen on the sides or ends of Au NRs was determined by the competition between electrostatic force and covalent binding of ligands. More complex assemblies can be generated when the presence of proteins is localized. For instance, gold-tipped CdSe NRs immobilized with avidin and biotin on the Au nanodomain organized into dimers, trimers, and flowers of NRs, depending on the ratio of biotin and avidin to NRs [138].

Ligand-guided assembly offers plenty of room for chemists to tune the assembly of 1D NCs. This method is easy to perform, and most of the assembly can be carried out in the solution phase without the use of any special instrument. The assembly of NCs is driven by interparticle forces that have great variety of directionality and specificity of interactions. Except for the use of DNA origami, the ligand-guided assembly usually does not offer good directionality as a field-driven assembly or high precision in the organization of NCs as templated assembly.

1.3 Properties and Applications

The assemblies of anisotropic 1D NCs often exhibit advanced or novel collective properties that are different from the individual NCs and their corresponding bulk counterparts. This is largely originated from the coupling interactions (e.g., plasmon–plasmon, dipole–dipole interactions, and coupling of magnetic moments) or synergistic effect between different components. As a result, these assemblies have showed great potential in a broad range of applications, such as chemical or biological sensing, nanoscale electronic and optoelectronic devices, information storage, and so on.

Noble metal NCs exhibit LSPR, which concentrates free-space electromagnetic waves within the regions close to the surfaces. The elongation of NCs to 1D morphology enables both transverse and longitudinal resonances that correspond to the confined oscillations oriented perpendicular and parallel to the long axis of the 1D NCs. Both transverse and longitudinal plasmon resonance can be tuned by controlling the aspect ratio of 1D NCs and, more importantly, by the presence of other neighboring NCs. Therefore, the arrangement and orientation of 1D NC arrays can be used to tune the surface plasmon coupling of NCs, triggering fascinating features [139]. Taking Au NRs as example, the placement of another Au NR in a close proximity will trigger different collective plasmon modes and provide a much larger field enhancement compared to the individual Au NRs [140]. El-Sayed *et al*. systematically studied the dependence of plasmonic coupling on the orientation/organization of Au NRs [80, 81]. The end-to-end linkage of Au NRs leads to a red shift of longitudinal LSPR band resulting from the attractive dipole coupling. In contrast, side-by-side assembly of Au NRs exhibits a blue shift of the longitudinal LSPR band and a red shift of the transverse LSPR band, as a result of the repulsive or attractive coupling of the corresponding plasmon modes [141]. This coupling phenomenon can be explained by exciton coupling theory, which can be viewed as the electromagnetic analogy of molecular orbitals (Figure 1.13a). In an end-to-end dimer, the

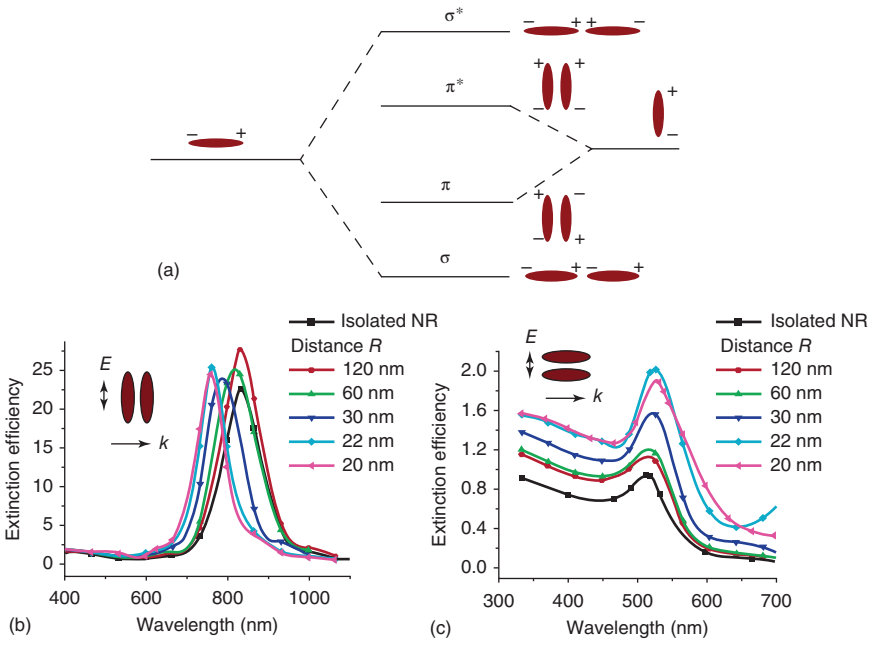

Figure 1.13 (a) Exciton theory picture of the essence of coupled longitudinal plasmon excitation in dimers of NRs. (b,c) Simulated (b) longitudinal and (c) transverse plasmon extinction efficiency spectra of Au NRs (length of 80 nm and width of 20 nm) assembled in a side-by-side orientation as a function of the inter-nanorod center-to-center distance. (Jain *et al*. 2006 [141]. Reproduced with permission of American Chemical Society.)

coupled longitudinal plasmon is analogous to the formation of σ-bond from two p_z orbitals, while in the side-by-side dimer the coupled longitudinal plasmon has an antibonding nature similar to the formation of a π* bond from $p_{x/y}$ orbitals. Moreover, the strength of plasmon coupling was found to increase with the shortening of the inter-rod distance, increasing number of interacting NRs and increasing the NR aspect ratio. Figure 1.13b,c illustrates the dependence of the longitudinal and transverse plasmon excitation on the center-to-center distance of NRs in a side-by-side orientation. Reasonable efforts have been devoted to understanding the dependence of plasmonic coupling on the assembly morphology of 1D NCs. The extreme sensitivity of plasmon coupling and the associated spectral response to interparticle distance and NC organization has been utilized for chemical and biological sensing, mainly based on triggering or preventing the self-assembly of NRs by the analyte [82, 137].

The coupling of 1D semiconductor NCs occurs mainly through Förster resonance energy transfer. The electronic coupling decreases with increasing center-to-center distance of NRs and is strongly dependent on the orientation of NRs. For instance, Franchini *et al.* studied the photoluminescence (PL) spectra of CdSe/CdS core–shell NRs with different alignments, that is, densely packed hexagonal arrays of vertically aligned NRs, laterally aligned ribbon-like

assemblies, and disordered NRs [61]. As shown in Figure 1.14, the PL spectrum of vertically oriented NRs is slightly blue-shifted compared to that of the ordered NRs. Ribbon-like assemblies of NRs exhibit a strong PL emission and an up to 30 MeV blue shift compared to disordered NRs. This difference in PL intensity between vertical and ribbon-like arrays of NRs is attributed to the spatial

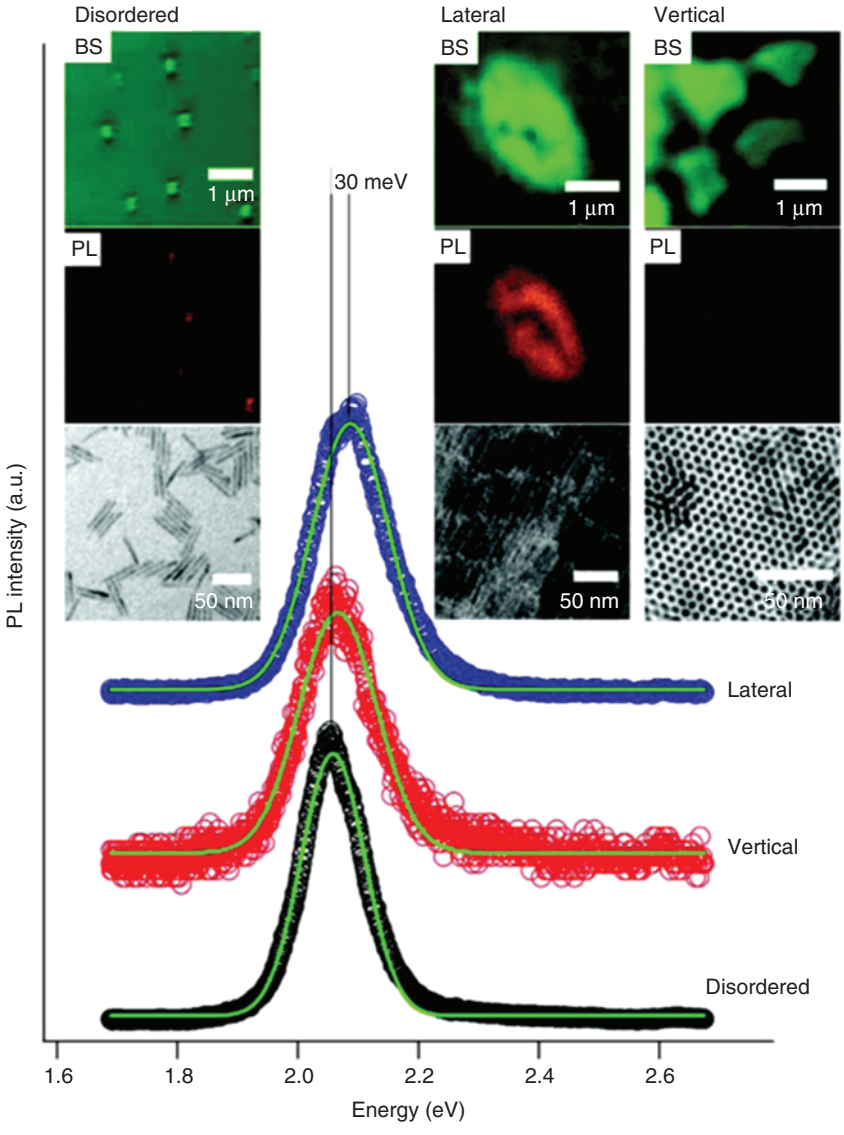

Figure 1.14 PL spectra of laterally and vertically aligned and disordered CdSe/CdS core–shell NRs with an aspect ratio of 10. The insets show the corresponding images of the laser backscattering and confocal setup and TEM images of the respective regions. (Carbone *et al*. 2007 [61]. Reproduced with permission of American Chemical Society.)

anisotropy of the optical dipole emission field of 1D NRs. Since the transition dipole is parallel to the long axis of the NR, the emission is maximum in the plane perpendicular to the dipole and minimum in the direction along its long axis.

Assemblies of magnetic NRs show potential applications in areas such as high-density information storage. A ferromagnetic or antiferromagnetic coupling is associated with the end-to-end or side-by-side organization of NRs [142]. The organization of NRs in 2D and 3D superlattice structures is expected to achieve a high packing density of NRs and hence a sufficiently large magnetic volume. For example, the superlattice of side-by-side aligned Co NRs perpendicular to the substrate exhibits a ferromagnetic feature at room temperature and a strong coercive field as a result of the large magnetic anisotropy of NRs [143]. This system has promising potential to be used in high-density magnetic recording.

1.4 Perspectives and Challenges

Self-assembly of 1D NCs has proven to be an efficient way to create a vast range of nanostructures with desired properties in a predetermined manner. Recent advances in the synthesis of NCs have offered us a large library of nanoscale building blocks for assembling functional materials, while development of novel assembly approaches enables one to exploit the properties and applications of these materials. However, the nonuniformity of building blocks has been always associated with the presence of defects within the assembled structures. It is crucial for researchers to understand the synthesis of NCs better and hence to further improve the uniformity of NCs. Moreover, current studies suggest that shape anisotropy of NCs plays an important role in the ordering of 1D NCs. It is also well known that chemical anisotropy of 1D NCs can very important in determining the specificity and directionality of NC organization. However, to date there has been few reports on controlling the chemical patches on the surface of 1D NCs [144, 145].

Second, despite the tremendous progress that has been made, more quantitative assessment and precise control of assembly structures are still in urgent need. Along this direction, more efforts should be made from at least the following aspects: (i) control over individual assemblies with single-particle precision; (ii) development of new approaches to control the initiation and termination of assembly process; and (iii) quantification of assembly structures at different assembly stages.

Third, well-ordered structures in a "zoom-in" area can only meet the need for characterization, but not for practical application. Future research should address the challenge in scaling up the assembly process to reproducibly produce large-area structures with minimum defects.

Finally, the combination of multiple fabrication approaches (e.g., top-down lithography and bottom-up assembly methods) might represent a new direction for controlling both short-range and long-range ordering of NCs. In this case, different forces associated with the organization of NCs need to be understood and controlled better.

References

1 Tao, A.R., Habas, S., and Yang, P. (2008) Shape control of colloidal metal nanocrystals. *Small*, **4** (3), 310–325.

2 Murray, C.B., Kagan, C., and Bawendi, M. (2000) Synthesis and characterization of monodisperse nanocrystals and close-packed nanocrystal assemblies. *Annu. Rev. Mater. Sci.*, **30** (1), 545–610.

3 Liu, K., Zhao, N., and Kumacheva, E. (2011) Self-assembly of inorganic nanorods. *Chem. Soc. Rev.*, **40** (2), 656–671.

4 Zhang, S.-Y., Regulacio, M.D., and Han, M.-Y. (2014) Self-assembly of colloidal one-dimensional nanocrystals. *Chem. Soc. Rev.*, **43** (7), 2301–2323.

5 Nie, Z. and Kumacheva, E. (2008) Patterning surfaces with functional polymers. *Nat. Mater.*, **7** (4), 277–290.

6 Jones, M.R., Osberg, K.D., Macfarlane, R.J., Langille, M.R., and Mirkin, C.A. (2011) Templated techniques for the synthesis and assembly of plasmonic nanostructures. *Chem. Rev.*, **111** (6), 3736–3827.

7 Geissler, M. and Xia, Y. (2004) Patterning: principles and some new developments. *Adv. Mater.*, **16** (15), 1249–1269.

8 van Blaaderen, A., Ruel, R., and Wiltzius, P. (1997) Template-directed colloidal crystallization. *Nature*, **385** (6614), 321–324.

9 Yin, Y., Lu, Y., Gates, B., and Xia, Y. (2001) Template-assisted self-assembly: a practical route to complex aggregates of monodispersed colloids with well-defined sizes, shapes, and structures. *J. Am. Chem. Soc.*, **123** (36), 8718–8729.

10 Kuemin, C., Nowack, L., Bozano, L., Spencer, N.D., and Wolf, H. (2012) Oriented assembly of gold nanorods on the single-particle level. *Adv. Funct. Mater.*, **22** (4), 702–708.

11 Thai, T., Zheng, Y., Ng, S.H., Mudie, S., Altissimo, M., and Bach, U. (2012) Self-assembly of vertically aligned gold nanorod arrays on patterned substrates. *Angew. Chem. Int. Ed.*, **51** (35), 8732–8735.

12 Flauraud, V., Mastrangeli, M., Bernasconi, G.D., Butet, J., Alexander, D.T.L., Shahrabi, E., Martin, O.J.F., and Brugger, J. (2016) Nanoscale topographical control of capillary assembly of nanoparticles. *Nat. Nanotechnol.*, **12**, 73–80. doi: 10.1038/nnano.2016.179

13 Hamon, C., Postic, M., Mazari, E., Bizien, T., Dupuis, C., Even-Hernandez, P., Jimenez, A., Courbin, L., Gosse, C., Artzner, F., and Marchi-Artzner, V. (2012) Three-dimensional self-assembling of gold nanorods with controlled macroscopic shape and local smectic B order. *ACS Nano*, **6** (5), 4137–4146.

14 Ahmed, S. and Ryan, K.M. (2007) Self-assembly of vertically aligned nanorod supercrystals using highly oriented pyrolytic graphite. *Nano Lett.*, **7** (8), 2480–2485.

15 Hamon, C., Novikov, S., Scarabelli, L., Basabe-Desmonts, L., and Liz-Marzan, L.M. (2014) Hierarchical self-assembly of gold nanoparticles into patterned plasmonic nanostructures. *ACS Nano*, **8** (10), 10694–10703.

16 Correa-Duarte, M.A., Perez-Juste, J., Sanchez-Iglesias, A., Giersig, M., and Liz-Marzan, L.M. (2005) Aligning an nanorods by using carbon nanotubes as templates. *Angew. Chem. Int. Ed.*, **44** (28), 4375–4378.
17 Merg, A.D., Boatz, J.C., Mandal, A., Zhao, G., Mokashi-Punekar, S., Liu, C., Wang, X., Zhang, P., van der Wel, P.C., and Rosi, N.L. (2016) Peptide-directed assembly of single-helical gold nanoparticle superstructures exhibiting intense chiroptical activity. *J. Am. Chem. Soc.*, **138** (41), 13655–13663.
18 Hore, M.J. and Composto, R.J. (2013) Functional polymer nanocomposites enhanced by nanorods. *Macromolecules*, **47** (3), 875–887.
19 Ferrier, R.C. Jr., Koski, J., Riggleman, R.A., and Composto, R.J. (2016) Engineering the assembly of gold nanorods in polymer matrices. *Macromolecules*, **49** (3), 1002–1015.
20 Hore, M.J. and Composto, R.J. (2010) Nanorod self-assembly for tuning optical absorption. *ACS Nano*, **4** (11), 6941–6949.
21 Deshmukh, R.D., Liu, Y., and Composto, R.J. (2007) Two-dimensional confinement of nanorods in block copolymer domains. *Nano Lett.*, **7** (12), 3662–3668.
22 Liu, Z.C., Huang, H.Y., and He, T.B. (2013) Large-area 2D gold nanorod arrays assembled on block copolymer templates. *Small*, **9** (4), 505–510.
23 Zhang, Q.L., Gupta, S., Emrick, T., and Russell, T.P. (2006) Surface-functionalized CdSe nanorods for assembly in diblock copolymer templates. *J. Am. Chem. Soc.*, **128** (12), 3898–3899.
24 Ploshnik, E., Salant, A., Banin, U., and Shenhar, R. (2010) Hierarchical surface patterns of nanorods obtained by Co-assembly with block copolymers in ultrathin films. *Adv. Mater.*, **22** (25), 2774–2779.
25 Thorkelsson, K., Nelson, J.H., Alivisatos, A.P., and Xu, T. (2013) End-to-end alignment of nanorods in thin films. *Nano Lett.*, **13** (10), 4908–4913.
26 Nepal, D., Onses, M.S., Park, K., Jespersen, M., Thode, C.J., Nealey, P.F., and Vaia, R.A. (2012) Control over position, orientation, and spacing of arrays of gold nanorods using chemically nanopatterned surfaces and tailored particle–particle–surface interactions. *ACS Nano*, **6** (6), 5693–5701.
27 Liu, Q., Senyuk, B., Tang, J., Lee, T., Qian, J., He, S., and Smalyukh, I.I. (2012) Plasmonic complex fluids of nematiclike and helicoidal self-assemblies of gold nanorods with a negative order parameter. *Phys. Rev. Lett.*, **109** (8), 088301.
28 Liu, Q., Campbell, M.G., Evans, J.S., and Smalyukh, I.I. (2014) Orientationally ordered colloidal co-dispersions of gold nanorods and cellulose nanocrystals. *Adv. Mater.*, **26** (42), 7178–7184.
29 Liu, Q.K., Cui, Y.X., Gardner, D., Li, X., He, S.L., and Smalyukh, I.I. (2010) Self-alignment of plasmonic gold nanorods in reconfigurable anisotropic fluids for tunable bulk metamaterial applications. *Nano Lett.*, **10** (4), 1347–1353.
30 Wang, L. and Li, Q. (2016) Stimuli-directing self-organized 3D liquid–crystalline nanostructures: from materials design to photonic applications. *Adv. Funct. Mater.*, **26** (1), 10–28.

31 Gharbi, M.A., Manet, S., Lhermitte, J., Brown, S., Milette, J., Toader, V., Sutton, M., and Reven, L. (2016) Reversible nanoparticle cubic lattices in blue phase liquid crystals. *ACS Nano*, **10** (3), 3410–3415.

32 Grzelczak, M., Vermant, J., Furst, E.M., and Liz-Marzán, L.M. (2010) Directed self-assembly of nanoparticles. *ACS Nano*, **4** (7), 3591–3605.

33 van der Zande, B.M., Koper, G.J., and Lekkerkerker, H.N. (1999) Alignment of rod-shaped gold particles by electric fields. *J. Phys. Chem. B*, **103** (28), 5754–5760.

34 Smith, P.A., Nordquist, C.D., Jackson, T.N., Mayer, T.S., Martin, B.R., Mbindyo, J., and Mallouk, T.E. (2000) Electric-field assisted assembly and alignment of metallic nanowires. *Appl. Phys. Lett.*, **77** (9), 1399.

35 Hu, Z., Fischbein, M.D., Querner, C., and Drndic, M. (2006) Electric-field-driven accumulation and alignment of CdSe and CdTe nanorods in nanoscale devices. *Nano Lett.*, **6** (11), 2585–2591.

36 Li, L.S. and Alivisatos, A.P. (2003) Origin and scaling of the permanent dipole moment in CdSe nanorods. *Phys. Rev. Lett.*, **90** (9), 097402.

37 Acharya, S., Patla, I., Kost, J., Efrima, S., and Golan, Y. (2006) Switchable assembly of ultra narrow CdS nanowires and nanorods. *J. Am. Chem. Soc.*, **128** (29), 9294–9295.

38 Ryan, K.M., Mastroianni, A., Stancil, K.A., Liu, H., and Alivisatos, A. (2006) Electric-field-assisted assembly of perpendicularly oriented nanorod superlattices. *Nano Lett.*, **6** (7), 1479–1482.

39 Huang, Z., Raciti, D., Yu, S., Zhang, L., Deng, L., He, J., Liu, Y., Khashab, N.M., Wang, C., and Gong, J. (2016) Synthesis of platinum nanotubes and nanorings via simultaneous metal alloying and etching. *J. Am. Chem. Soc.*, **138** (20), 6332–6335.

40 Gupta, S., Zhang, Q., Emrick, T., and Russell, T.P. (2006) "Self-corralling" nanorods under an applied electric field. *Nano Lett.*, **6** (9), 2066–2069.

41 Englander, O., Christensen, D., Kim, J., Lin, L., and Morris, S.J. (2005) Electric-field assisted growth and self-assembly of intrinsic silicon nanowires. *Nano Lett.*, **5** (4), 705–708.

42 Singh, J.P., Lele, P.P., Nettesheim, F., Wagner, N.J., and Furst, E.M. (2009) One-and two-dimensional assembly of colloidal ellipsoids in ac electric fields. *Phys. Rev. E*, **79** (5), 050401.

43 Wang, K., Jin, S.M., Xu, J.P., Liang, R.J., Shezad, K., Xue, Z.G., Xie, X.L., Lee, E., and Zhu, J.T. (2016) Electric-field-assisted assembly of polymer-tethered gold nanorods in cylindrical nanopores. *ACS Nano*, **10** (5), 4954–4960.

44 Wang, M., He, L., and Yin, Y. (2013) Magnetic field guided colloidal assembly. *Mater. Today*, **16** (4), 110–116.

45 Tanase, M., Bauer, L.A., Hultgren, A., Silevitch, D.M., Sun, L., Reich, D.H., Searson, P.C., and Meyer, G.J. (2001) Magnetic alignment of fluorescent nanowires. *Nano Lett.*, **1** (3), 155–158.

46 Chen, M., Pica, T., Jiang, Y.-B., Li, P., Yano, K., Liu, J.P., Datye, A.K., and Fan, H. (2007) Synthesis and self-assembly of fcc phase FePt nanorods. *J. Am. Chem. Soc.*, **129** (20), 6348–6349.

47 Anagnostopoulou, E., Grindi, B., Lacroix, L.-M., Ott, F., Panagiotopoulos, I., and Viau, G. (2016) Dense arrays of cobalt nanorods as rare-earth free permanent magnets. *Nanoscale*, **8** (7), 4020–4029.

48 Ding, T., Song, K., Clays, K., and Tung, C.H. (2009) Fabrication of 3D photonic crystals of ellipsoids: convective self-assembly in magnetic field. *Adv. Mater.*, **21** (19), 1936–1940.

49 Yan, J., Chaudhary, K., Bae, S.C., Lewis, J.A., and Granick, S. (2013) Colloidal ribbons and rings from Janus magnetic rods. *Nat. Commun.*, **4**, 1516.

50 Huang, Y., Duan, X., Wei, Q., and Lieber, C.M. (2001) Directed assembly of one-dimensional nanostructures into functional networks. *Science*, **291** (5504), 630–633.

51 Liu, J.-W., Liang, H.-W., and Yu, S.-H. (2012) Macroscopic-scale assembled nanowire thin films and their functionalities. *Chem. Rev.*, **112** (8), 4770–4799.

52 Kuhn, P., Puigmartí-Luis, J., Imaz, I., Maspoch, D., and Dittrich, P.S. (2011) Controlling the length and location of in situ formed nanowires by means of microfluidic tools. *Lab Chip*, **11** (4), 753–757.

53 Zhou, H., Heyer, P., Kim, H.-J., Song, J.-H., Piao, L., and Kim, S.-H. (2011) Reversible macroscopic alignment of Ag nanowires. *Chem. Mater.*, **23** (16), 3622–3627.

54 Wang, L., Liu, Y., He, J., Hourwitz, M.J., Yang, Y., Fourkas, J.T., Han, X., and Nie, Z. (2015) Continuous microfluidic self-assembly of hybrid Janus-like vesicular motors: autonomous propulsion and controlled release. *Small*, **11** (31), 3762–3767.

55 Pickering, S.U. (1907) CXCVI.—emulsions. *J. Chem. Soc. Trans.*, **91**, 2001–2021.

56 Ramsden, W. (1903) Separation of solids in the surface-layers of solutions and 'suspensions' (observations on surface-membranes, bubbles, emulsions, and mechanical coagulation) – preliminary account. *Proc. R. Soc. Lond.*, **72**, 156–164.

57 Pieranski, P. (1980) Two-dimensional interfacial colloidal crystals. *Phys. Rev. Lett.*, **45** (7), 569.

58 Dong, L. and Johnson, D.T. (2005) Adsorption of acicular particles at liquid-fluid interfaces and the influence of the line tension. *Langmuir*, **21** (9), 3838–3849.

59 Basavaraj, M., Fuller, G., Fransaer, J., and Vermant, J. (2006) Packing, flipping, and buckling transitions in compressed monolayers of ellipsoidal latex particles. *Langmuir*, **22** (15), 6605–6612.

60 Lewandowski, E.P., Searson, P.C., and Stebe, K.J. (2006) Orientation of a nanocylinder at a fluid interface. *J. Phys. Chem. B*, **110** (9), 4283–4290.

61 Carbone, L., Nobile, C., De Giorgi, M., Sala, F.D., Morello, G., Pompa, P., Hytch, M., Snoeck, E., Fiore, A., and Franchini, I.R. (2007) Synthesis and micrometer-scale assembly of colloidal CdSe/CdS nanorods prepared by a seeded growth approach. *Nano Lett.*, **7** (10), 2942–2950.

62 Rizzo, A., Nobile, C., Mazzeo, M., Giorgi, M.D., Fiore, A., Carbone, L., Cingolani, R., Manna, L., and Gigli, G. (2009) Polarized light emitting diode

by long-range nanorod self-assembling on a water surface. *ACS Nano*, **3** (6), 1506–1512.

63 Sánchez-Iglesias, A., Rivas-Murias, B., Grzelczak, M., Pérez-Juste, J., Liz-Marzán, L.M., Rivadulla, F., and Correa-Duarte, M.A. (2012) Highly transparent and conductive films of densely aligned ultrathin Au nanowire monolayers. *Nano Lett.*, **12** (12), 6066–6070.

64 Sánchez-Iglesias, A., Grzelczak, M., Pérez-Juste, J., and Liz-Marzán, L.M. (2010) Binary self-assembly of gold nanowires with nanospheres and nanorods. *Angew. Chem. Int. Ed.*, **49** (51), 9985–9989.

65 Khanal, B.P. and Zubarev, E.R. (2007) Rings of nanorods. *Angew. Chem. Int. Ed.*, **46** (13), 2195–2198.

66 Tao, A., Kim, F., Hess, C., Goldberger, J., He, R., Sun, Y., Xia, Y., and Yang, P. (2003) Langmuir–Blodgett silver nanowire monolayers for molecular sensing using surface-enhanced Raman spectroscopy. *Nano Lett.*, **3** (9), 1229–1233.

67 Tao, A.R., Huang, J., and Yang, P. (2008) Langmuir–Blodgettry of nanocrystals and nanowires. *Acc. Chem. Res.*, **41** (12), 1662–1673.

68 Kim, F., Kwan, S., Akana, J., and Yang, P. (2001) Langmuir–Blodgett nanorod assembly. *J. Am. Chem. Soc.*, **123** (18), 4360–4361.

69 Acharya, S., Panda, A.B., Belman, N., Efrima, S., and Golan, Y. (2006) A semiconductor-nanowire assembly of ultrahigh junction density by the Langmuir–Blodgett technique. *Adv. Mater.*, **18** (2), 210–213.

70 Whang, D., Jin, S., Wu, Y., and Lieber, C.M. (2003) Large-scale hierarchical organization of nanowire arrays for integrated nanosystems. *Nano Lett.*, **3** (9), 1255–1259.

71 Liu, J.-W., Zhu, J.-H., Zhang, C.-L., Liang, H.-W., and Yu, S.-H. (2010) Mesostructured assemblies of ultrathin superlong tellurium nanowires and their photoconductivity. *J. Am. Chem. Soc.*, **132** (26), 8945–8952.

72 Yang, P. and Kim, F. (2002) Langmuir–Blodgett assembly of one-dimensional nanostructures. *ChemPhysChem*, **3** (6), 503–506.

73 Böker, A., He, J., Emrick, T., and Russell, T.P. (2007) Self-assembly of nanoparticles at interfaces. *Soft Matter*, **3** (10), 1231–1248.

74 Singh, A., Gunning, R.D., Ahmed, S., Barrett, C.A., English, N.J., Garate, J.-A., and Ryan, K.M. (2012) Controlled semiconductor nanorod assembly from solution: influence of concentration, charge and solvent nature. *J. Mater. Chem.*, **22** (4), 1562–1569.

75 Ming, T., Kou, X., Chen, H., Wang, T., Tam, H.L., Cheah, K.W., Chen, J.Y., and Wang, J. (2008) Ordered gold nanostructure assemblies formed by droplet evaporation. *Angew. Chem.*, **120** (50), 9831–9836.

76 Ghezelbash, A., Koo, B., and Korgel, B.A. (2006) Self-assembled stripe patterns of CdS nanorods. *Nano Lett.*, **6** (8), 1832–1836.

77 Koster, L.J.A., Khodabakhsh, S., and Greenham, N.C. (2014) Controlling the assembly of CdS nanorods via solvent and acidity. *Soft Matter*, **10** (34), 6485–6490.

78 Zanella, M., Gomes, R., Povia, M., Giannini, C., Zhang, Y., Riskin, A., Van Bael, M., Hens, Z., and Manna, L. (2011) Self-assembled multilayers of vertically aligned semiconductor nanorods on device-scale areas. *Adv. Mater.*, **23** (19), 2205–2209.

79 Baker, J.L., Widmer-Cooper, A., Toney, M.F., Geissler, P.L., and Alivisatos, A.P. (2009) Device-scale perpendicular alignment of colloidal nanorods. *Nano Lett.*, **10** (1), 195–201.

80 Shibu Joseph, S., Ipe, B.I., Pramod, P., and Thomas, K.G. (2006) Gold nanorods to nanochains: mechanistic investigations on their longitudinal assembly using α,ω-alkanedithiols and interplasmon coupling. *J. Phys. Chem. B*, **110** (1), 150–157.

81 Thomas, K.G., Barazzouk, S., Ipe, B.I., Joseph, S.S., and Kamat, P.V. (2004) Uniaxial plasmon coupling through longitudinal self-assembly of gold nanorods. *J. Phys. Chem. B*, **108** (35), 13066–13068.

82 Sudeep, P., Joseph, S.S., and Thomas, K.G. (2005) Selective detection of cysteine and glutathione using gold nanorods. *J. Am. Chem. Soc.*, **127** (18), 6516–6517.

83 Sun, Z., Ni, W., Yang, Z., Kou, X., Li, L., and Wang, J. (2008) pH-Controlled reversible assembly and disassembly of gold nanorods. *Small*, **4** (9), 1287–1292.

84 Wang, Y., DePrince, A.E. III, Gray, S.K., Lin, X.-M., and Pelton, M. (2010) Solvent-mediated end-to-end assembly of gold nanorods. *J. Phys. Chem. Lett.*, **1** (18), 2692–2698.

85 Chan, Y.T., Li, S., Moorefield, C.N., Wang, P., Shreiner, C.D., and Newkome, G.R. (2010) Self-assembly, disassembly, and reassembly of gold nanorods mediated by bis(terpyridine)–metal connectivity. *Chem. Eur. J.*, **16** (14), 4164–4168.

86 Park, H.-S., Agarwal, A., Kotov, N.A., and Lavrentovich, O.D. (2008) Controllable side-by-side and end-to-end assembly of Au nanorods by lyotropic chromonic materials. *Langmuir*, **24** (24), 13833–13837.

87 Leung, F.C.-M., Leung, S.Y.-L., Chung, C.Y.-S., and Yam, V.W.-W. (2016) Metal–metal and π–π interactions directed end-to-end assembly of gold nanorods. *J. Am. Chem. Soc.*, **138** (9), 2989–2992.

88 Wang, T., Zhuang, J., Lynch, J., Chen, O., Wang, Z., Wang, X., LaMontagne, D., Wu, H., Wang, Z., and Cao, Y.C. (2012) Self-assembled colloidal superparticles from nanorods. *Science*, **338** (6105), 358–363.

89 Baranov, D., Fiore, A., van Huis, M., Giannini, C., Falqui, A., Lafont, U., Zandbergen, H., Zanella, M., Cingolani, R., and Manna, L. (2010) Assembly of colloidal semiconductor nanorods in solution by depletion attraction. *Nano Lett.*, **10** (2), 743–749.

90 Talapin, D.V., Shevchenko, E.V., Murray, C.B., Kornowski, A., Förster, S., and Weller, H. (2004) CdSe and CdSe/CdS nanorod solids. *J. Am. Chem. Soc.*, **126** (40), 12984–12988.

91 Abécassis, B. (2016) Three-dimensional self assembly of semiconducting colloidal nanocrystals: from fundamental forces to collective optical properties. *ChemPhysChem*, **17** (5), 618–631.

92 Taniguchi, Y., Takishita, T., Kawai, T., and Nakashima, T. (2016) End-to-end self-assembly of semiconductor nanorods in water by using an amphiphilic surface design. *Angew. Chem.*, **128** (6), 2123–2126.

93 Kim, D., Kim, W.D., Kang, M.S., Kim, S.-H., and Lee, D.C. (2014) Self-organization of nanorods into ultra-long range two-dimensional monolayer end-to-end network. *Nano Lett.*, **15** (1), 714–720.

94 Huang, H.-C., Koria, P., Parker, S.M., Selby, L., Megeed, Z., and Rege, K. (2008) Optically responsive gold nanorod–polypeptide assemblies. *Langmuir*, **24** (24), 14139–14144.

95 González-Rubio, G., González-Izquierdo, J., Bañares, L., Tardajos, G., Rivera, A., Altantzis, T., Bals, S., Peña-Rodríguez, O., Guerrero-Martínez, A., and Liz-Marzán, L.M. (2015) Femtosecond laser-controlled tip-to-tip assembly and welding of gold nanorods. *Nano Lett.*, **15** (12), 8282–8288.

96 He, L., Zhang, L., Ye, Y., and Liang, H. (2010) Solvent-induced self-assembly of polymer-tethered nanorods. *J. Phys. Chem. B*, **114** (21), 7189–7200.

97 Zhuang, J., Shaller, A.D., Lynch, J., Wu, H., Chen, O., Li, A.D., and Cao, Y.C. (2009) Cylindrical superparticles from semiconductor nanorods. *J. Am. Chem. Soc.*, **131** (17), 6084–6085.

98 Zhang, Z., Horsch, M.A., Lamm, M.H., and Glotzer, S.C. (2003) Tethered nano building blocks: toward a conceptual framework for nanoparticle self-assembly. *Nano Lett.*, **3** (10), 1341–1346.

99 Marson, R.L., Nguyen, T.D., and Glotzer, S.C. (2015) Rational design of nanomaterials from assembly and reconfigurability of polymer-tethered nanoparticles. *MRS Commun.*, **5** (03), 397–406.

100 Horsch, M.A., Zhang, Z., and Glotzer, S.C. (2005) Self-assembly of polymer-tethered nanorods. *Phys. Rev. Lett.*, **95** (5), 056105.

101 Horsch, M.A., Zhang, Z., and Glotzer, S.C. (2006) Simulation studies of self-assembly of end-tethered nanorods in solution and role of rod aspect ratio and tether length. *J. Chem. Phys.*, **125** (18), 184903.

102 Iacovella, C.R., Horsch, M.A., and Glotzer, S.C. (2008) Local ordering of polymer-tethered nanospheres and nanorods and the stabilization of the double gyroid phase. *J. Chem. Phys.*, **129** (4), 044902.

103 Horsch, M.A., Zhang, Z., and Glotzer, S.C. (2010) Self-assembly of end-tethered nanorods in a neat system and role of block fractions and aspect ratio. *Soft Matter*, **6** (5), 945–954.

104 Horsch, M.A., Zhang, Z., and Glotzer, S.C. (2006) Self-assembly of laterally-tethered nanorods. *Nano Lett.*, **6** (11), 2406–2413.

105 Nguyen, T.D. and Glotzer, S.C. (2009) Switchable helical structures formed by the hierarchical self-assembly of laterally tethered nanorods. *Small*, **5** (18), 2092–2098.

106 Nguyen, T.D. and Glotzer, S.C. (2010) Reconfigurable assemblies of shape-changing nanorods. *ACS Nano*, **4** (5), 2585–2594.

107 Nie, Z., Fava, D., Kumacheva, E., Zou, S., Walker, G.C., and Rubinstein, M. (2007) Self-assembly of metal–polymer analogues of amphiphilic triblock copolymers. *Nat. Mater.*, **6** (8), 609–614.

108 Liu, K., Nie, Z., Zhao, N., Li, W., Rubinstein, M., and Kumacheva, E. (2010) Step-growth polymerization of inorganic nanoparticles. *Science*, **329** (5988), 197–200.

109 Lukach, A., Liu, K., Therien-Aubin, H., and Kumacheva, E. (2012) Controlling the degree of polymerization, bond lengths, and bond angles of plasmonic polymers. *J. Am. Chem. Soc.*, **134** (45), 18853–18859.

110 Liu, K., Resetco, C., and Kumacheva, E. (2012) Salt-mediated kinetics of the self-assembly of gold nanorods end-tethered with polymer ligands. *Nanoscale*, **4** (20), 6574–6580.

111 Liu, K., Lukach, A., Sugikawa, K., Chung, S., Vickery, J., Therien-Aubin, H., Yang, B., Rubinstein, M., and Kumacheva, E. (2014) Copolymerization of metal nanoparticles: a route to colloidal plasmonic copolymers. *Angew. Chem. Int. Ed.*, **53** (10), 2648–2653.

112 Song, J., Cheng, L., Liu, A., Yin, J., Kuang, M., and Duan, H. (2011) Plasmonic vesicles of amphiphilic gold nanocrystals: self-assembly and external-stimuli-triggered destruction. *J. Am. Chem. Soc.*, **133** (28), 10760–10763.

113 Song, J., Pu, L., Zhou, J., Duan, B., and Duan, H. (2013) Biodegradable theranostic plasmonic vesicles of amphiphilic gold nanorods. *ACS Nano*, **7** (11), 9947–9960.

114 He, J., Wei, Z., Wang, L., Tomova, Z., Babu, T., Wang, C., Han, X., Fourkas, J.T., and Nie, Z. (2013) Hydrodynamically driven self-assembly of giant vesicles of metal nanoparticles for remote-controlled release. *Angew. Chem. Int. Ed.*, **52** (9), 2463–2468.

115 Huang, Z., Liu, Y., Zhang, Q., Chang, X., Li, A., Deng, L., Yi, C., Yang, Y., Khashab, N.M., and Gong, J. (2016) Collapsed polymer-directed synthesis of multicomponent coaxial-like nanostructures. *Nat. Commun.*, **7**, 12147.

116 Nykypanchuk, D., Maye, M.M., van der Lelie, D., and Gang, O. (2008) DNA-guided crystallization of colloidal nanoparticles. *Nature*, **451** (7178), 549–552.

117 Macfarlane, R.J., Lee, B., Jones, M.R., Harris, N., Schatz, G.C., and Mirkin, C.A. (2011) Nanoparticle superlattice engineering with DNA. *Science*, **334** (6053), 204–208.

118 Leunissen, M.E., Dreyfus, R., Cheong, F.C., Grier, D.G., Sha, R., Seeman, N.C., and Chaikin, P.M. (2009) Switchable self-protected attractions in DNA-functionalized colloids. *Nat. Mater.*, **8** (7), 590–595.

119 Zhang, Y., Lu, F., Yager, K.G., van der Lelie, D., and Gang, O. (2013) A general strategy for the DNA-mediated self-assembly of functional nanoparticles into heterogeneous systems. *Nat. Nanotechnol.*, **8** (11), 865–872.

120 Wang, Y., Wang, Y., Zheng, X., Ducrot, É., Yodh, J.S., Weck, M., and Pine, D.J. (2015) Crystallization of DNA-coated colloids. *Nat. Commun.*, **6**, 7253.

121 Zhang, Y., Pal, S., Srinivasan, B., Vo, T., Kumar, S., and Gang, O. (2015) Selective transformations between nanoparticle superlattices via the reprogramming of DNA-mediated interactions. *Nat. Mater.*, **14** (8), 840–847.

122 Jones, M.R., Macfarlane, R.J., Lee, B., Zhang, J., Young, K.L., Senesi, A.J., and Mirkin, C.A. (2010) DNA-nanoparticle superlattices formed from anisotropic building blocks. *Nat. Mater.*, **9** (11), 913–917.

123 Li, Z., Zhu, Z., Liu, W., Zhou, Y., Han, B., Gao, Y., and Tang, Z. (2012) Reversible plasmonic circular dichroism of Au nanorod and DNA assemblies. *J. Am. Chem. Soc.*, **134** (7), 3322–3325.

124 Vial, S., Nykypanchuk, D., Yager, K.G., Tkachenko, A.V., and Gang, O. (2013) Linear mesostructures in DNA–nanorod self-assembly. *ACS Nano*, **7** (6), 5437–5445.

125 Tørring, T., Voigt, N.V., Nangreave, J., Yan, H., and Gothelf, K.V. (2011) DNA origami: a quantum leap for self-assembly of complex structures. *Chem. Soc. Rev.*, **40** (12), 5636–5646.

126 Tian, Y., Wang, T., Liu, W., Xin, H.L., Li, H., Ke, Y., Shih, W.M., and Gang, O. (2015) Prescribed nanoparticle cluster architectures and low-dimensional arrays built using octahedral DNA origami frames. *Nat. Nanotechnol.*, **10** (7), 637–644.

127 Hung, A.M., Micheel, C.M., Bozano, L.D., Osterbur, L.W., Wallraff, G.M., and Cha, J.N. (2010) Large-area spatially ordered arrays of gold nanoparticles directed by lithographically confined DNA origami. *Nat. Nanotechnol.*, **5** (2), 121–126.

128 Lan, X., Chen, Z., Dai, G., Lu, X., Ni, W., and Wang, Q. (2013) Bifacial DNA origami-directed discrete, three-dimensional, anisotropic plasmonic nanoarchitectures with tailored optical chirality. *J. Am. Chem. Soc.*, **135** (31), 11441–11444.

129 Shen, C., Lan, X., Lu, X., Ni, W., and Wang, Q. (2015) Tuning the structural asymmetries of three-dimensional gold nanorod assemblies. *Chem. Commun.*, **51** (71), 13627–13629.

130 Rao, C., Wang, Z.-G., Li, N., Zhang, W., Xu, X., and Ding, B. (2015) Tunable optical activity of plasmonic dimers assembled by DNA origami. *Nanoscale*, **7** (20), 9147–9152.

131 Schreiber, R., Luong, N., Fan, Z., Kuzyk, A., Nickels, P.C., Zhang, T., Smith, D.M., Yurke, B., Kuang, W., and Govorov, A.O. (2013) Chiral plasmonic DNA nanostructures with switchable circular dichroism. *Nat. Commun.*, **4**, Article number: 2948.

132 Jiang, Q., Shi, Y., Zhang, Q., Li, N., Zhan, P., Song, L., Dai, L., Tian, J., Du, Y., and Cheng, Z. (2015) A self-assembled DNA origami-gold nanorod complex for cancer theranostics. *Small*, **11** (38), 5134–5141.

133 Du, Y., Jiang, Q., Beziere, N., Song, L., Zhang, Q., Peng, D., Chi, C., Yang, X., Guo, H., and Diot, G. (2016) DNA-nanostructure–gold-nanorod hybrids for enhanced in vivo optoacoustic imaging and photothermal therapy. *Adv. Mater.*, **28**, 10000–10007.

134 Maune, H.T., Han, S.-P., Barish, R.D., Bockrath, M., III Goddard, W.A., Rothemund, P.W., and Winfree, E. (2010) Self-assembly of carbon nanotubes into two-dimensional geometries using DNA origami templates. *Nat. Nanotechnol.*, **5** (1), 61–66.

135 Lan, X., Lu, X., Shen, C., Ke, Y., Ni, W., and Wang, Q. (2014) Au nanorod helical superstructures with designed chirality. *J. Am. Chem. Soc.*, **137** (1), 457–462.

136 Caswell, K., Wilson, J.N., Bunz, U.H., and Murphy, C.J. (2003) Preferential end-to-end assembly of gold nanorods by biotin-streptavidin connectors. *J. Am. Chem. Soc.*, **125** (46), 13914–13915.

137 Wang, L., Zhu, Y., Xu, L., Chen, W., Kuang, H., Liu, L., Agarwal, A., Xu, C., and Kotov, N.A. (2010) Side-by-side and end-to-end gold nanorod assemblies for environmental toxin sensing. *Angew. Chem. Int. Ed.*, **49** (32), 5472–5475.

138 Salant, A., Amitay-Sadovsky, E., and Banin, U. (2006) Directed self-assembly of gold-tipped CdSe nanorods. *J. Am. Chem. Soc.*, **128** (31), 10006–10007.

139 Huang, X., Neretina, S., and El-Sayed, M.A. (2009) Gold nanorods: from synthesis and properties to biological and biomedical applications. *Adv. Mater.*, **21** (48), 4880–4910.

140 Chen, H., Shao, L., Li, Q., and Wang, J. (2013) Gold nanorods and their plasmonic properties. *Chem. Soc. Rev.*, **42** (7), 2679–2724.

141 Jain, P.K., Eustis, S., and El-Sayed, M.A. (2006) Plasmon coupling in nanorod assemblies: optical absorption, discrete dipole approximation simulation, and exciton-coupling model. *J. Phys. Chem. B*, **110** (37), 18243–18253.

142 Dumestre, F., Chaudret, B., Amiens, C., Respaud, M., Fejes, P., Renaud, P., and Zurcher, P. (2003) Unprecedented crystalline super-lattices of monodisperse cobalt nanorods. *Angew. Chem. Int. Ed.*, **42** (42), 5213–5216.

143 Wetz, F., Soulantica, K., Respaud, M., Falqui, A., and Chaudret, B. (2007) Synthesis and magnetic properties of Co nanorod superlattices. *Mater. Sci. Eng. C*, **27** (5), 1162–1166.

144 Singh, C., Hu, Y., Khanal, B.P., Zubarev, E.R., Stellacci, F., and Glotzer, S.C. (2011) Striped nanowires and nanorods from mixed SAMS. *Nanoscale*, **3** (8), 3244–3250.

145 Choueiri, R.M., Galati, E., Thérien-Aubin, H., Klinkova, A., Larin, E.M., Querejeta-Fernández, A., Han, L., Xin, H.L., Gang, O., and Zhulina, E.B. (2016) Surface patterning of nanoparticles with polymer patches. *Nature*, **538**, 79–83.